Alma Mater Studiorum – Università di Bologna

DOTTORATO DI RICERCA IN

MECCANICA E SCIENZE AVANZATE DELL'INGEGNERIA

Ciclo 33

Settore Concorsuale: 09/A2 – MECCANICA APPLICATA ALLE MACCHINE

Settore Scientifico Disciplinare: ING-IND/13 – MECCANICA APPLICATA ALLE MACCHINE

OPTIMAL DESIGN OF COMPLIANT ACTUATORS

Presentata da: Guido Bocchieri

Coordinatore Dottorato

Marco Carricato

Supervisore

Rocco Vertechy

Co-supervisore

Vincenzo Parenti Castelli

Luca Luzi

Esame finale anno 2021

When you wanna give up
and your heart's about to break
Remember that you're perfect
God makes no mistakes.
Welcome to wherever you are
This is your life, you made it this far!
Welcome, you got to believe
Right here, right now you're exactly
where you're supposed to be.
J. B. Jovi

Contents

List of Figures

List of Tables

Optimal Design of Compliant Actuators

Application to a Differential Elastic Actuator

Guido Bocchieri

Abstract

Compliant actuators are mechanical devices that extend the traditional architecture of robotic joints (motor – transmission – load) by introducing in the power transmission chain some degree of compliance, in the form of off-the-shelf springs or elastic and deformable components. Depending on where and how these compliant elements are inserted in the transmission, many different architectures of compliant actuators arise. The objective of this work is to analyze these different architectures from a theoretical point of view, derive new optimal design techniques and methodologies and, finally, apply these techniques to design new prototypes of robotic actuators devoted to specific applications.

Optimal Design of Compliant Actuators

Application to a Differential Elastic Actuator

Guido Bocchieri

Abstract

Gli attuatori elastici sono dispositivi meccanici che estendono l'architettura tradizionale dei giunti robotici (motore - riduttore - carico) introducendo nella catena di trasmissione del moto un certo grado di cedevolezza, sotto forma di molle commerciali o componenti ad-hoc elastici e deformabili. A seconda di dove e come questi componenti sono inseriti nella trasmissione molteplici architetture di attuatori elastici vengono a formarsi. L'obiettivo di questo lavoro è analizzare queste diverse architetture da un punto di vista teorico, derivare nuove tecniche e metodologie di progettazione ottimizzate e, infine, applicare queste linee guida alla progettazione vera e propria di nuovi prototipi di attuatori robotici dedicati ad applicazioni specifiche.

Chapter 1

Literature Review

Typically robots are employed in structured, known environments, performing tasks requiring precise movement in space. This is normally achieved taking advantage both on a rigid mechanical assembly and through high-gain control loops. Typical industrial tasks that fall into this category are welding, spray painting, pick-and-place. Such stiff architectures, however, are not suited for other apparently trivial tasks that require any kind of interaction with the environment, which can be also totally or partially unknown, such as assembly, surface finishing, quality inspection. Moreover, such stiff architectures pose a serious safety threat to humans since no collaboration (or even spatial proximity) with operators is allowed. This kind of interaction requires a change in the control paradigm: robots require force control instead of position control.

This Chapter introduces the main fundamental concepts involved in the design of robotic applications that require controlled interaction: the necessity of force control, and the importance of compliance. Different solutions to actively and passively introduce compliance in robotic applications are presented. Finally, some commonly known architectures of compliant robotic actuators are introduced.

Chapter 2 deals with the mathematical modeling of compliant actuators. Both the forward and inverse dynamics problems are stated, and the relevance of their solution for several engineering tasks (simulation, control, optimization) is explained. The fundamental components of common robotic actuators are presented and modeled, together with an innovative modeling of linear and rotational compliant springs. The previously presented actuator architectures are analyzed in a general and unified framework. For each one, the solution of the direct and inverse dynamics problem is formulated.

Chapter 3 starts with the traditional procedure to optimize the power transmission chain of rigid actuators. The traditional procedure is then ex-

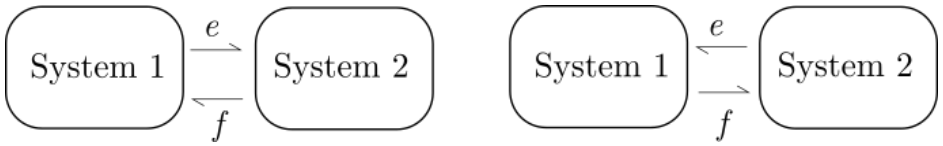

Figure 1.1: Each system can only control either the effort or the flow at the interface

Domain	Effort	Flow
Mechanical translation	Force	Velocity
Mechanical rotation	Torque	Angular Velocity
Hydraulic	Pressure	Volume flow rate
Electric	Voltage	Current

Table 1.1: Effort and flow variables in different domains

tended to cope with the multi-degree of freedom nature of compliant actuators. Examples of design optimization are presented in different application scenarios for two different, widely used, compliant actuator architectures.

Chapter 4 introduces the the design of an optimized Differential Elastic Actuator empowered with a braking mechanism.

1.1 Force Control

When the task to be performed requires interaction, the robot needs the capability to measure and control forces, together with joint positions. The robot needs to know where its end-effector is, but also how it is interfacing with its surrounding.

The answer to the problem, which will be the key topic throughout all this work, which is *compliance*, arises from a simple physical analysis of how two independent systems interact at the energetic level. A thorough discussion on the concept of causality, and how this influences the interaction between systems, can be found in [4], together with an in depth description of the bond-graph theory for system physical modeling.

It turns out that in any energetic domain (mechanical translational and rotational, electrical, hydraulic, etc.) the interaction between two systems is governed by two variables, *effort* and *flow*, whose product is the power (measured in Watts), transferred between the two systems. For example, in the mecahnical translational domain the effort variable is the force (F) and the flow variable is the velocity (v). Other examples of effort-flow variables can be found in Table 1.1.

A very important consequence is that physical systems cannot control both these interface variables simultaneously, but only one at a time, as schematized in Figure 1.1. Any kind of interaction between two entities, and this is true for both engineering systems and human relations, occurs as a mutual exchange of something: both entities need to participate in this phenomenon, giving and taking at the same time. Intuitively, from an energetic point of view, if a system was able to control both effort and flows at an interface this would mean that it would be able to control, and thus generate, arbitrary power (and therefore energy).

To understand why this is important, let's consider a simple example, the contact between a robot's end-effector and a surface (for example, a wall). Usually, objects which robots need to interact with are kinematically constrained, for example a wall imposes the constraint that the velocity along its perpendicular direction is zero. Therefore, it is clear that the system "wall" imposes the flow variable (velocity) at the interface, and as a consequence the end-effector can only impose the effort variable (force). The problem is that robots are normally position-controlled, meaning that they can schematized as pure *flow* sources: this poses a fundamental physical incompatibility between the two systems, since they are both trying to control the *flow* at the interface, as shown in Figure 1.2a.

The causality issue can be solved in two different ways:

1. Switching to a *force-controlled* scheme. This means that the robot does not control the position of the EE, but the force exerted on the EE by the environment. This adds complexity to the system, since force needs to be measured (either directly, with load cells for example) or indirectly (as in SEAs and other compliant actuators, measuring the deflection of some compliant material). In this context, the EE becomes an effort source, and the resulting bond graph:

$$S_e \dashv 1 \vdash S_f$$

   despite being physically trivial, is correct from the causal point of view.

2. Introducing compliance in the mechanism. This switches the scenario from Figure 1.2a to Figure 1.2b. The compliance at the interface between the EE and the wall enables both systems to control the flow at their interface, whereas the effort, the force, is imposed by the deflection of the elastic component.

It's important to notice that what is depicted in Figure 1.2b is what actually happens in reality if we try to position-control the interaction of a

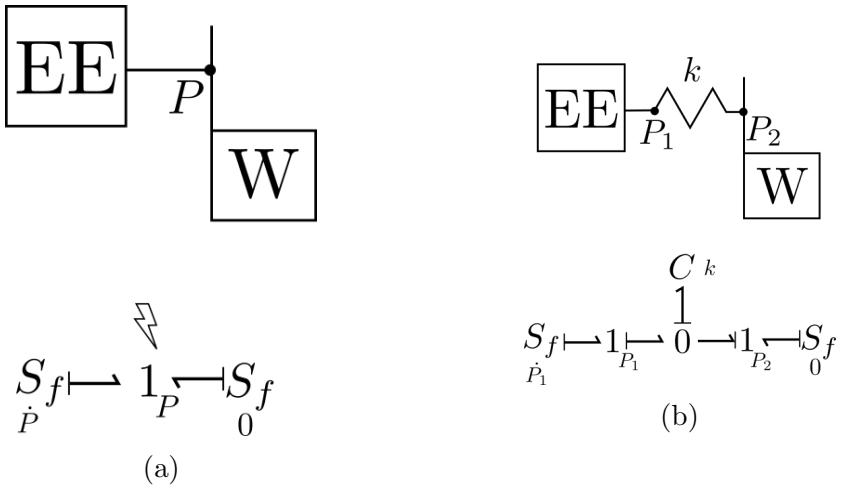

Figure 1.2: (a) Causality issue: both systems impose the flow variable at the interface (b) No causal issue is present if compliance is added. The presence of compliance solves the causality issues, meaning that this is the correct physical interpretation of the interaction. The stiffness k can be either the interface's material inherent compliance, or an added compliance in either of the two systems

robot EE with a constrained surface, but the elasticity at the interface is given by the materials of which the EE and the surface are made of, which usually is quite high and therefore hardly controllable. If we deliberately insert some form of compliance in the transmission, for example on the EE, we achieve the same result, which is shock-tolerance and decoupling of the two interfaces, but we can choose the compliance and tune it accordingly to the application, thus reducing the robot's output impedance.

1.2 Interaction with the environment

The correct execution of a task requiring interaction with the environment employing standard motion control algorithms would require a perfect planning of the movements. A perfect, detailed, knowledge of the kinematics and dynamics of the robot and the geometry and mechanical characteristics of the environment would be of paramount importance. Albeit the former would be reasonably possible, it's not always feasible to assume perfect knowledge of an unstructured, possibly time varying, environment.

As an example, in typical mechanical assembling tasks driven by pure position control it's necessary to guarantee the relative position of compo-

nents with a precision that is at least one order of magnitude grater than the required assembly tolerance.

In practice, errors generate contact forces that cause deviations from the nominal, desired trajectory. At the same time, the controller is designed to react and eliminate such deviations (let's think of a simple PI controller). This escalation often leads to an uncontrolled increase of the contact forces, that usually ends due to either saturation of the actuators or mechanical damage to one of the components involved (either in the robot or in the environment).

What's worse is that such unstable interaction is more likely to happen the higher is the stiffness of the environment and the higher is the stiffness of the control algorithm.

Such unstable escalation can only be overcome ensuring compliant behavior during interaction. It should be clear the the contact force is the key variable to monitor the interaction, and therefore at least intuitively it's reasonable to expect that measuring such quantity and using it somehow in the control algorithm would lead to better results during the interaction phase.

Interaction stabilization strategies can be classified into two macro categories:

1. *Passive*: where the intervention is mainly on the mechanical structure of the robot and/or the environment

2. *Active*: where the intervention is mainly on the control algorithms and actuator/sensor architecture.

Active methods can be further subdivided in *Indirect* methods, that obtain force control through motion control, and *Direct*, where contact force is measured and a force loop is closed, possibly in a cascaded architecture, together with other control loops.

1.2.1 Passive Compliance

A simple but effective technique to empower the robot with (sort-of) force control is to continue using position control architectures but incorporate passive compliance in the transmission. Compliance can be injected in the robot itself, either in the links or at the joints, or in the end-effector.

In this scenario, no measurement of the interaction effort is employed at the control level, therefore no force feedback is present in the architecture.

This achieves a similar effect of lowering the total closed loop position controller gain. The reduced stiffness deriving from a more compliant mechanical structure and a less rigid control algorithm might enable the robot

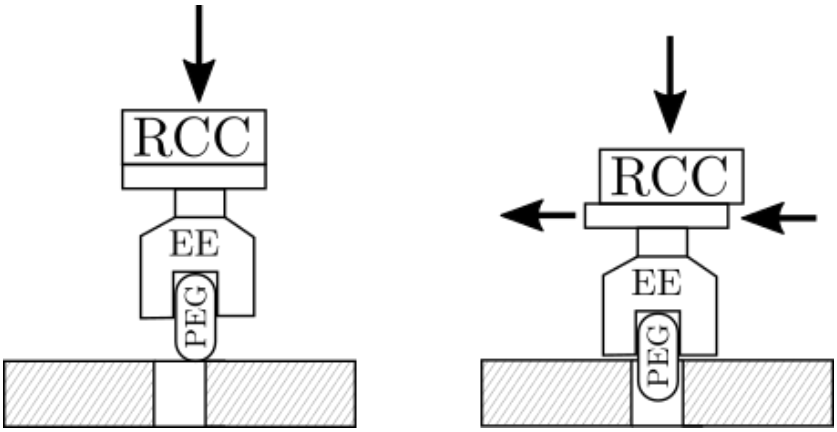

Figure 1.3: Remote Center of Compliance employed in a typical peg-in-the-hole task. The misalignment is automatically adjusted by the device itself, without any modification of the EE trajectory

to successfully manage the interaction with the environment without shocks, impacts and damages of any kind. However this comes at the cost of reduced precision and efficiency in performing the necessary task. Inaccuracy comes from the compliance in the links and/or actuators, which cannot be directly compensated by the control loop, since measurement of such deviations is hardly ever possible. Inefficiency comes from the lowering of the total control loop gain, which would cause increasing of the settling time and/or increased overshoot also in a non-compliant scenarios.

A possibility to add compliance is to employ pneumatic actuation, that exploits the natural compressibility of gases. The control system is devoted to control the gas pressure in the pneumatic cylinder, that gets converted into output force.

Another possibility to mitigate the downsides of pure passive compliance is to inject compliance only at the end effector level. This comes from the consideration that robots usually interact with the environment only at specific endpoints.

Therefore, the robot can approximately position the tool's endpoint in the unconstrained environment as usual, employing stiff mechanical structure and high gain position control loops, and then slowly perform the interaction task taking advantage of compliance at the interface, such as rubber covering. This is similar to what happens in nature, for example with human hands, whose surface is covered by a compliant skin, that compensates for inaccurate positioning and increases shock tolerance.

A similar, widely used technique is the remote center of compliance

(RCC), whose working principle is schematized in Figure 1.3. These devices, that usually are inserted between the robot's wrist and the end effector, prevent peg-like objects to jam while being inserted in holes with tight tolerances, due to inaccuracies of the end effector's positioning.

RCCs make sure that contact forces arising from misalignments move the peg in such a way to correct the issue, instead of worsening it, making sure that those forces acting on the compliance center result in pure translation and torques at that point cause pure rotation [6].

1.2.2 Active Compliance

To achieve active compliance, peculiar control schemes have been developed to enhance or substitute the classic position control loops. Active compliance can be achieved either directly, measuring and closing a force control loop, or indirectly, possibly measuring the contact force but closing a position control loop.

Among indirect force control schemes we recall:

1. *Stiffness Control* This scheme does not make use of force feedback measurement, but tunes the control gains in order to achieve different dynamics responses in each movement direction of the EE. In a typical application the EE can be constrained in some directions (for example in the *approach* direction, with respect to the interaction surface) but not in the others. Therefore, the control gains can be tuned in order to achieve high rigidity in some non-constrained directions and achieve the desired level of compliance, to be matched with the compliance of the environment, in the constrained directions.

2. *Impedance Control* The position and velocity of the robot endpoint is commanded to follow some trajectory. In addition, the control system imposes a second order mass-spring-damper behavior between contact forces and the robot's position, velocity and acceleration. In other words, the robot endpoint will behave as if it is a second order system. Therefore the endpoint forces, joint positions and velocities are used to generate actuator torques. The gain matrices which set the effective stiffness, damping and inertia of the manipulator endpoint can be selected depending on the desired behavior.

Among direct force control schemes we recall:

1. *Pure Force Control* This architecture eliminates the position information from the loop. Only force measurements are used as controlled

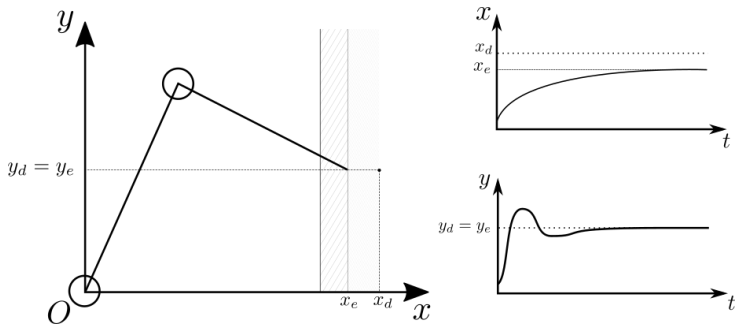

Figure 1.4: Stiffness control applied to a 2 DOF planar serial manipulator during interaction with a compliant environment. Control is stiff in the y, non-constrained direction, and compliant in the x, constrained direction. The final y_e position equals the commanded one y_d, whereas the final x_e position depends on the stiffness of the control as well as the stiffness of the environment.

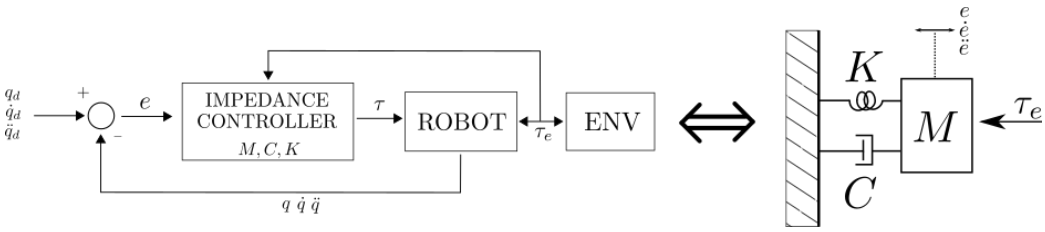

Figure 1.5: Scheme of impedance control. The closed loop system is equivalent to an N-DOF second order mass-spring-damper system, whose dynamics can be tuned according to requirements.

variables, and a desired interface force is used as a setpoint. This control scheme therefore transforms the robot from a pure position servo to a pure force servo. The controller input is the error between the desired interface force and the measured one. Since there is no positional feedback employed, there is no direct control on absolute endpoint position.

2. *Force control with inner position/velocity loop* In this architecture there is an inner, pre-existing control loop that regulates either the position or the velocity of the EE. This architecture presents the same disadvantages as the pure force control loop, but enables a finer tuning of the dynamic response of the closed loop system.

3. *Parallel force/position control* This control scheme is similar to the force control with inner position loop case, but an additional input

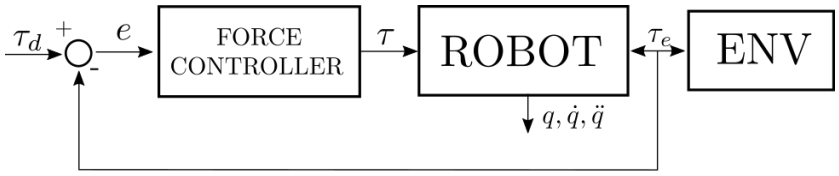

Figure 1.6: Scheme of pure force control. Only the contact force measurement is used as feedback source.

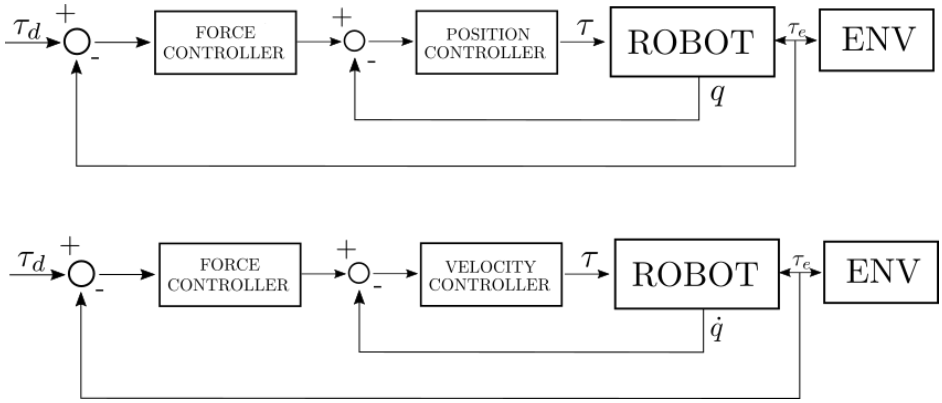

Figure 1.7: Scheme of cascaded control with external force loop and internal position/velocity loop.

variable is considered. The higher level controller can specify both the desired interface force and the desired EE position. Therefore, in the direction where unconstrained motion is allowed, the controller is still able to perform the task with high performances. On the contrary, along directions where motion is constrained by the environment, the additional desired EE position is seen as an additional disturbance. The presence of integral action in the force controller ensures that the desired interface force is reached at steady state, at the expense of a positioning error dependent on the compliance of the environment.

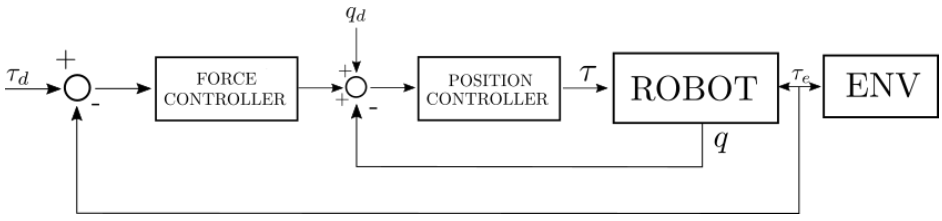

Figure 1.8: Scheme of parallel force-position control.

1.3 Compliant Robot Actuators

Typical robot joints employ electro-magnetic motors as their main actuation devices. This is not the only method though:

1. Hydraulic
2. Pneumatic
3. Shape memory alloy
4. Dielectric elastomers

Each actuation method has strengths and weaknesses with respect to force control, force density and power density. The main issue that makes all of them non ideal for interaction tasks is that those with high force and high power density typically have also high impedance. Therefore these actuators are difficult to use in force control situations regardless of sensory feedback information.

In an attempt to overcome this issues, it is possible to decouple the dynamics of the actuator from that of the robot by placing a compliant element between the two. This gives passive compliance to the actuators. In addition, by measuring the deflection of the spring, an estimate of force in the joint is obtained and can be used for active feedback control.

Introducing compliance into the drive system is contrary to conventional machine design mantra, which has always followed the golden rule "the stiffer the better". Traditionally, machines and drive systems are built to be as stiff as possible to increase bandwidth and accuracy.

However, it is interesting to note that the archetypal actuator for force control, biological muscle, is connected in series to a link output (the bone) through an elastic tendon [1]. The reason behind this is probably higher energy storage and increased effciency, stability when contacting environments and filtering shock loads to the body.

Elastic elements can be useful to actuation regardless of whether the system is biological or aritficial. Active measurement of the deflection of a compliant element in an actuator can provide an indirect measurement of the interaction force exchanged with the environment, together with the aforementioned benefits. This is the idea behind Series Elastic Actuators.

1.4 Series Elastic Actuators

The first to adopt the idea of inserting a compliant element in the power transmission was Howard [10]. His actuator featured a mechanical spring in

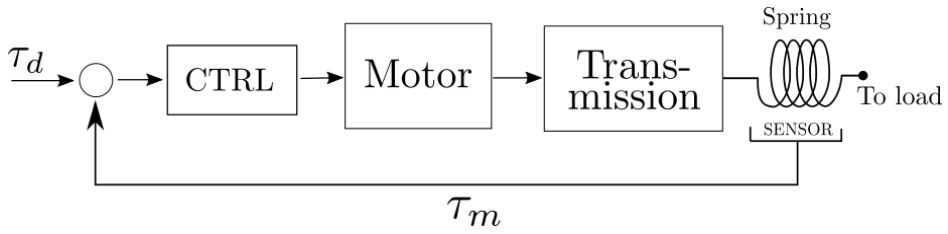

Figure 1.9: Series Elastic Actuator. A spring is places right at the interface of the actuator, between the load and the motor/transmission chain. The deflection of the spring is measured and fed back to the controller, as an indirect output torque's measurement.

series with an electric motor and a transmission. Two encoders measured the motor's angular position and output shaft's angular position. The spring's deflection was indirectly measured taking the difference between the two measurements.

From Hooke's law:

$$F = k\Delta x \tag{1.1}$$

it follows that controlling the spring's deflection means actually controlling the actuator's output torque.

Pratt and Williamson [9, 30] then showed that using an indirect, differential measurement for the spring's deflection introduces non negligible error due to the transmission compliance and backlash, in particular with high stiffness springs that induces small deflections, thus making the overall measurement too noisy. The typical architecture is shown in Figure 1.9. It was shown that directly measuring the strain of the spring led to better force measurement that resulted in higher quality force control, while still retaining friction and backlash filtering, typical of high transmissions, and impact shock loading from the environment.

After the first prototypes, several iterations of actuators or entire robots have been designed employing the Series Elastic Actuator concept:

- *COG*: COG, presented in Figure 1.10, is a humanoid robot with upper torso and head [23]. Each arm has 6 degrees of freedom, actuated by Series Elastic Actuators.

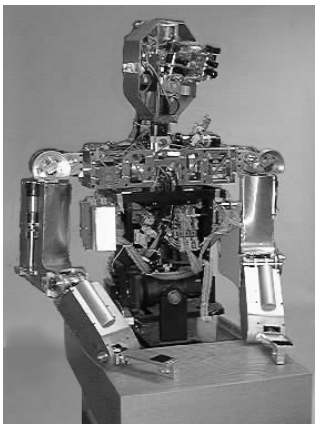

Figure 1.10: COG humanoid robot

- *Spring Flamingo*: Spring Flamingo, shown in Figure 1.11, is a planar bipedal walking robot with series elastic actuators driving six degrees of freedom [20] (three in each leg for hip, knee and ankle). Its walking speed is 1.25 m/s on flat terrain, as well as uneven uphill or downhill terrain with up to 15° slope.

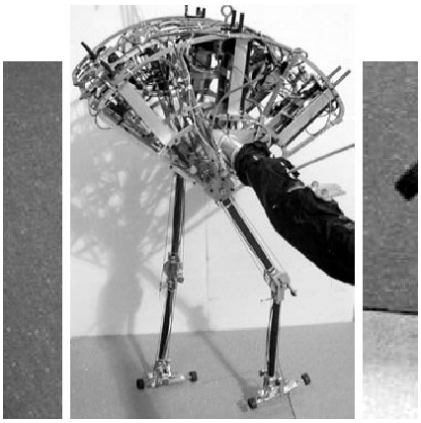

Figure 1.11: Spring Flamingo legged robot

- *M2*: M2, Figure 1.12, is a 3 dimensional bipedal walking robot. It has 12 degrees of freedom, 3 at each hip, 1 at each knee and 2 at each ankle [22]. Each joint is actuated with a Series Elastic Actuator. The robot is capable of walking at the speed of 1 m/s, climbing normal stairs and turning dynamically.

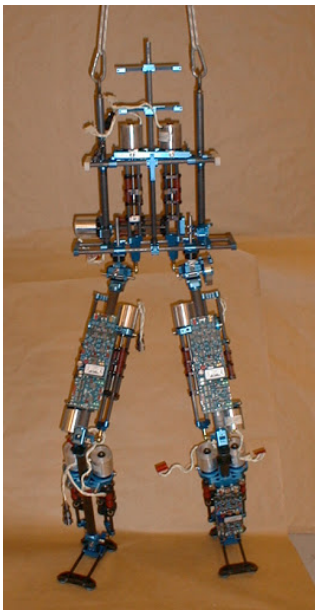

Figure 1.12: M2 legged robot

- *Baxter*: Baxter is a commercial industrial collaborative robot. It features two arms equipped with Series Elastic Actuators and an animated face as shown in Figure 1.13. It is intended to be employed in production sites side by side with human operators for simple jobs such as loading, unloading, sorting, handling, grasping and assembling. It can be easily programmed by directly moving its joints by hand to learn and perform a given repetitive task.

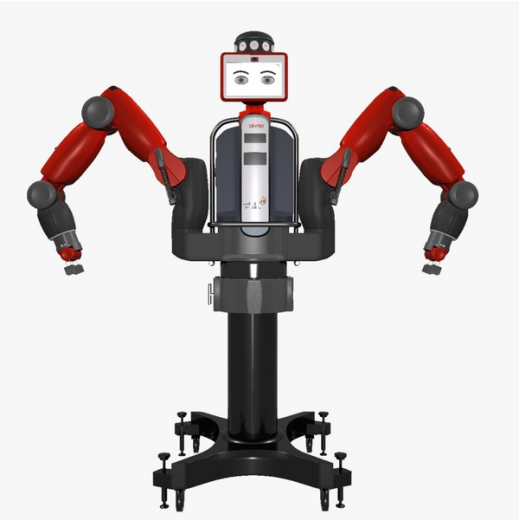

Figure 1.13: Baxter robot

- *Valkyrie*: NASA-JSC's Valkyrie Humanoid Robot, shown in Figure 1.14, has 44 actuated degrees of freedom, together with a set of sensors including stereo vision, laser range fingers, sonar depth perception, and tactile feedback [19].
  Each upper arm consists of 4 series elastic rotary actuators and when combined with the forearm has 7 joints. Each upper leg contains five series elastic rotary actuators. The ankle is realized using two series elastic linear actuators working in concert. The robot's torso houses two series elastic rotary actuators (the first arm joint on either side), two series elastic linear actuators that work in concert to realize motion between the torso and pelvis. The pelvis houses three series elastic rotary actuators: the waist rotation joint, and the hip rotation joint of each leg.

Figure 1.14: NASA-JSC's Valkyrie Humanoid Robot

The concept of Series Elastic Actuation revolves around the idea of adding to the traditional components of a standard actuator, a motor and a transmission, a third component, the compliance, in series. In the first formulation the elastic element resides after the transmission, right at the interface of the actuator. Nonetheless, in the years many different architectures have been proposed. In [14], an interesting classification is proposed. Series Elastic Actuators are classified in three categories according to the relative position of the spring with respect to the transmission, as in Figure 1.18:

1. Force-sensing Series Elastic Actuator (FSEA) which locates the spring after the transmission. Therefore, the spring can directly measure the force from the load. This is the original architecture presented for SEAs. The motor stator is directly attached to ground and provides an absolute effort. The transmission then amplifies this effort. The balance between the external effort and the amplified motor effort drives the deformation of the spring. External efforts directly affect the spring, that thus acts as a low-pass filter for shocks and impacts. Figure 1.15 shows two examples of FSEA. Figure 1.15a is the first SEA implemented in [9]. Figure 1.15b shows the SEA designed in [2] : a prosthetic ankle that matches size and weight of the human ankle. Active force control on such device enhances the capability of mimicking the human gait.

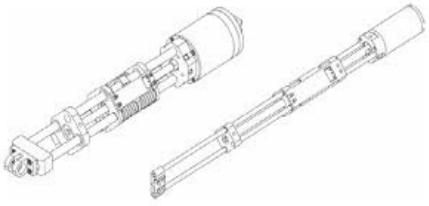

(a) Original SEA prototype

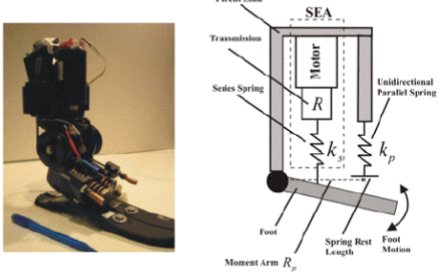

(b) SEA employed as ankle prosthetic device

Figure 1.15: Force-sensing Series Elastic Actuator (FSEA)

2. Reaction Force-sensing Series Elastic Actuator (RFSEA) which locates the spring before the transmission. Therefore the spring can be placed in two different positions: between the ground and the motor stator, or between the motor rotor and the transmission. In the first case the motor generates a relative effort between stator and rotor that gets directly amplified by the transmission and transferred to the load. The spring deformation is proportional to the reaction force of the motor with respect to ground. In the second case the spring deflection measures directly the balance between the motor effort and the reduced external effort. An example of the first type of RFSEA is shown in Figure 1.16. The design, presented in [18], uses a pulley and a ballscrew to generate prismatic motion from a rotating DC motor. A compression spring is mounted between the motor stator and ground, and its deflection is measured using an encoder and a pulley subsystem to convert linear motion back to rotational.

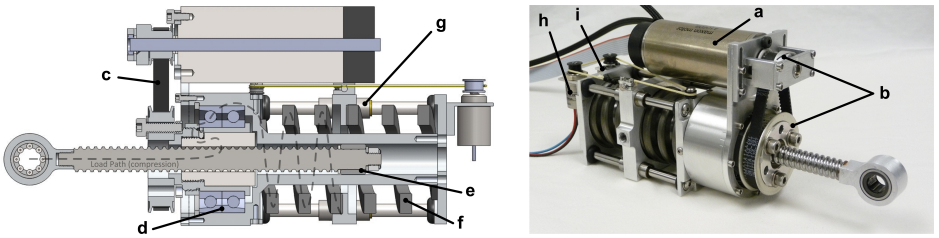

Figure 1.16: Reaction Force-sensing Series Elastic Actuator (RFSEA)

3. Transmitted Force-sensing Series Elastic Actuator (TFSEA) which locates the spring inside the transmission. To implement this idea, often

differential transmission (such as planetary gearing, harmonic drives or cycloidal gearing) is employed since it allows the connection of three entities (input-output-housing) to the transmission, instead of the usual two (input-output) of normal gears. For this reason, actuators belonging to this category are often reffered to as Differential Elastic Actuators. In this configuration, the motor effort is transmitted to the load through one path in the differential transmission and at the same time the external effort is transmitted to the gear housing and discharged to ground through the spring, and can thus be measured. Two examples of this architecture are presented in Figure 1.17. Figure 1.17a shows a planetary geared elastic actuator presented in [13]: the motor torque is transmitted from the sun gear to the carrier that is connected to the load, whereas the torque in the transmission can be measured by means of a spring connected between the ring gear and the ground. Figure 1.17b shows the DEA constructed with a Harmonic Drive as differential transmission, presented in [12]: the motor torque acts on the wave generator while the load is connected to the circular spline. The flexible spline is connected to ground through a torsional spring.

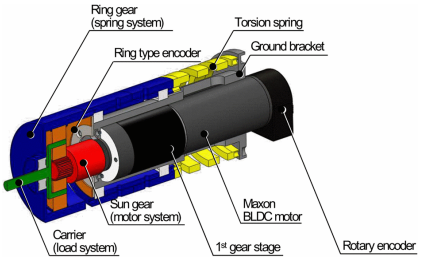

(a) TFSEA with planetary gearbox

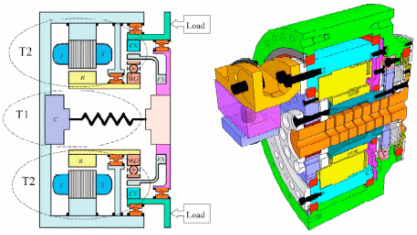

(b) TFSEA (DEA) constructed employing Harmonic Drive and hollow-shaft motor

Figure 1.17: Transmitted Force-sensing Series Elastic Actuator (TFSEA)

1.5 Parallel Elastic Actuators

Another class of actuators employing compliant elements is PEAs, Parallel Elastic Actuators. Differently from SEAs, PEAs are 1-DOF devices. There is no explicit decoupling of input and output of the actuator. The compliance is placed in parallel with respect to the transmission and is used as a storage of potential energy. The stored energy can be released acting in parallel with the motor, reducing consequently its torque demand. An example application

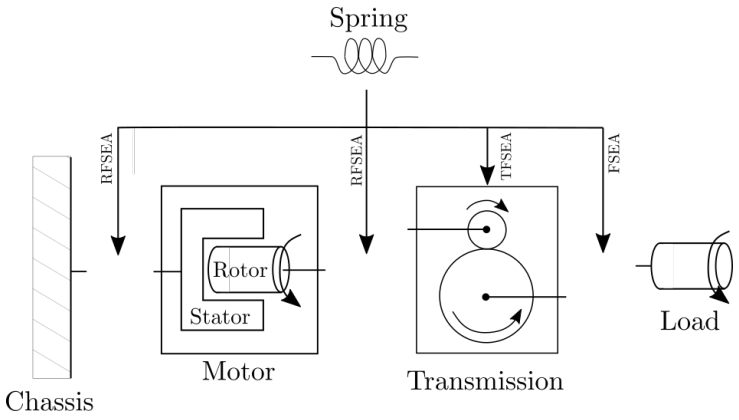

Figure 1.18: The position of the spring determines different Series Elastic Actuators architectures

can be found in [26], where a PEA is designed for a back-support exoskeleton at the hip joint, as depicted in Figure 1.19.

The implementation of the mechanical spring is realized through a bungee cable. The key aspect in designing PEAs is the consideration of the equilibrium angle of the spring, that is the motor angle with respect to ground at which the spring exerts zero torque. This is something that is usually neglected in SEAs, since the spring exerts torque based on the difference between two moving axes, motor and load, but is of paramount importance in PEAs since one of the two spring ends is connected to ground and thus it is fixed.

1.6 Variable Impedance Actuators

The SEAs presented in the previous sections incorporate a compliant element whose elasticity is fixed: it must be selected at design stage depending on the application. If a different elasticity is needed for a different application, the spring subsystem must be redesigned.

Variable Stiffness Actuators are devices that incorporate compliant elements as well in their architecture, but feature also some additional mechanisms by means of which the overall impedance of the actuator can be modified at runtime. This often means the addition of another actuator inside the device, since now two quantities must be controlled at the same time, the position and the impedance. Despite VIAs are not considered in this work, they're worth mentioning since these devices have received great attention in recent years and many variations and implementations have been proposed.

(a)

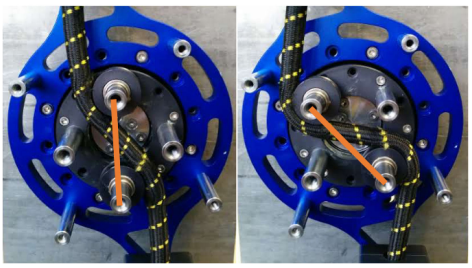

(b)

Figure 1.19: (a) PEA based hip joint for lower limb exoskeleton (b) The PEA joint presented in [26]. Near the equilibrium position the bungee exerts zero torque on the actuator. When the actuator moves in one direction under the combined action of human motion and gravity (the movement is then "assisted" by gravity) the bungee is loaded and accumulates potential energy, that can be given back during motion in opposite direction

A comprehensive classification and discussion on the state of the art can be found in [28] and the subsequent white papers by the same authors.

The main technological solutions that allow the runtime modification of the actuator's impedance are shown in Figure 1.20 and can be classified as:

1. *Nonlinear springs*: Equation 1.1 is valid only if the spring's stiffness is linear. Once k is defined, the compliant element exerts a torque proportional to the displacement of its ends, and the overall impedance of the actuator is defined once and for all. If the torque-displacement curve on the other hand was not linear, the overall impedance of the actuator would be dependent on the positional displacement of the actuator: such springs can be designed depending on the application for repetitive positioning tasks, in order to have low impedance during steps of the trajectory where compliance is needed, and high impedance where compliance is not needed. Spring non-linearity can be obtained both at manufacturing time (springs that have nonlinear torque-displacement characteristics by design) or employing linear springs with a nonlinear output mechanism (for example, through cam profiles).

2. *Preload adjustment of single spring*: We saw that in PEAs one crucial design aspect is the spring's equilibrium position, which is defined once and for all at assembly time, since one end is connected to the mechanism's ground. If instead that end of the spring was connected

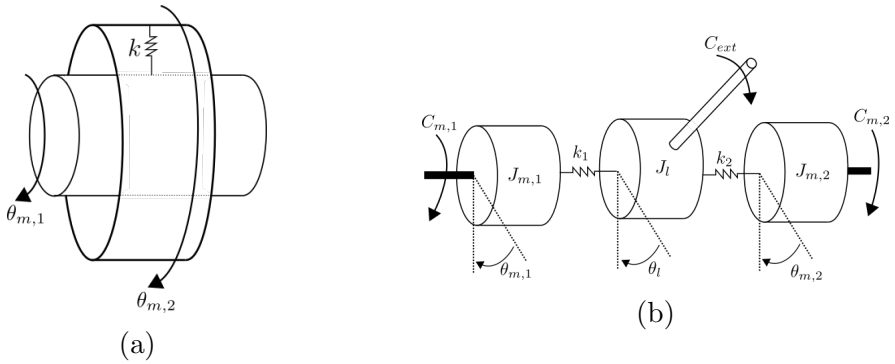

Figure 1.20: (a) Preload adjustment: the second motor regulates the equilibrium position of the spring. (b) Agonist-antagonist principle: two SEAs in parallel are capable to regulate both motion and impedance of the actuator.

to a moving element, controlled by a second motor, as shown in Figure 1.20a, we could achieve the same result of employing nonlinear springs, using only a single linear spring and an additional actuator. The control of this supplementary actuator would allow to change at runtime the preloading condition of the spring, thus realizing any desired impedance (withing physical boundaries of the components).

3. *Agonist-antagonist principle:* Mimicking the biological principle of antagonist muscles, for which the stronger the antagonistic forces, the stiffer the articulation becomes, these actuators are made up of two antagonist SEAs with nonlinear springs, kinematically in parallel with respect to the load. Intuitively, common-mode motion of the two actuators produces motion at the output, whereas differential-mode motion produces preloading on the springs without output motion. The combination of common and differential motion, imposed by ad-hoc control algorithms, can control both actuator motion and impedance at the interface. A diagram of the architecture is presented in Figure 1.20b.

1.7 Variable Damping Actuator

As mentioned in previous sections, compliance has been recognized as the key, enabling feature to empower robots with the necessary capabilities to successfully carry on tasks requiring interaction with humans and/or the environment. However, compliance also introduces some drawbacks, as the introduction of oscillatory behavior which can seriously decrease the accu-

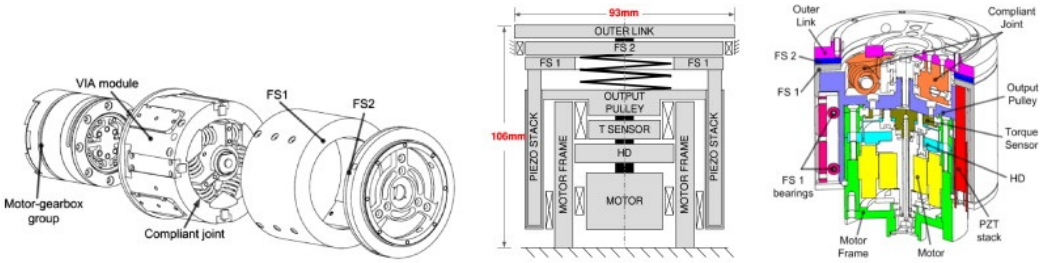

Figure 1.21: The variable damping actuator presented in [11]. Damping is realized with two friction surfaces made in Kevlar, whose relative movement is regulated with a piezoelectric actuator.

racy, stability of the robot, reducing its closed-loop bandwidth. This issues can only partially be dealt with using state-of-the-art control algorithms.

Taking again inspiration from bio-mechanical structure of mammalian muscles, that allow varying the level of joint damping during motion in order to achieve the desired behavior [16], a particularly interesting solution to the problem of uncontrolled oscillations is the introduction of, possibly controlled, damping at the interface between motor and joint, in parallel with the compliant element. Two different implementations of this concept are presented in [11, 5].

As will be shown in Chapter 2, viscous damping can always be introduced in the mathematical model of actuators, mainly due to friction due to bearings and surface contact. The idea is to introduce on purpose a certain amount of damping in the transmission, similar to the idea of introducing compliance that gave rise to the SEA concept, and control it according to the required task. For example, damping could be kept small at beginning of motion, in order to reduce energy dissipation and increase shock-tolerance in case of collision, and increased near the setpoint, where velocities would be smaller and less dangerous anyway, in order to damp oscillation and reduce settling time and overshoot typical of oscillatory motion.

Variable damping can be implemented in various ways, among which we mention:

1. Magnetorheological (MR) fluids [5], that produce viscous-like torque when subject to magnetic field, generated for example with an electrified coil.

2. Friction surfaces [11], where a second actuator (for example, a piezoelectric actuator) controls the engagement/disengagement and the pressure between two friction surfaces, one fixed and the other tied to the output link. When disengaged, the actuator works as a normal SEA

without additional damping. When engaged, friction is injected, and controlled, between the output link and the actuator's ground. The implementation proposed in [11] is presented in Figure 1.21.

Chapter 2

Mathematical modeling

In this chapter the fundamental mathematical tools needed for analysis, design, optimization, and eventually control of compliant actuators are presented. The main components of an actuator are presented and modeled. A method to take into consideration also the elastic element's self-inertia (which is commonly neglected) is presented. The single elementary models are then joined together to form the more complex actuators' models.

The dynamics equations for several categories of actuators are derived and a general method, easily extensible to other possible architectures, is presented. A general procedure to solve both the direct (for analysis and simulation) and the inverse (for design and optimization) dynamics problem is also presented.

2.1 Introduction

Proper mathematical modeling of compliant actuators is necessary for many reasons: control laws development, mechanism analysis, component optimization and simulation. All these problems require the solution of the mechanism's dynamic equations, both in the direct and inverse scenarios:

- *Direct dynamic problem*: Fixed the parameter vector γ and the external efforts $C_{ext}(t)$, given the time evolution of the input control variables (E.g. motor torque ($C_m(t)$), solve for the kinematic quantities $q(t)$, $\dot{q}(t)$, ... This enables the designer to simulate the physical behavior of the actuator.

- *Inverse dynamic problem*: Fixed the parameter vector γ and the external efforts $C_{ext}(t)$, given the desired time evolution of the motion

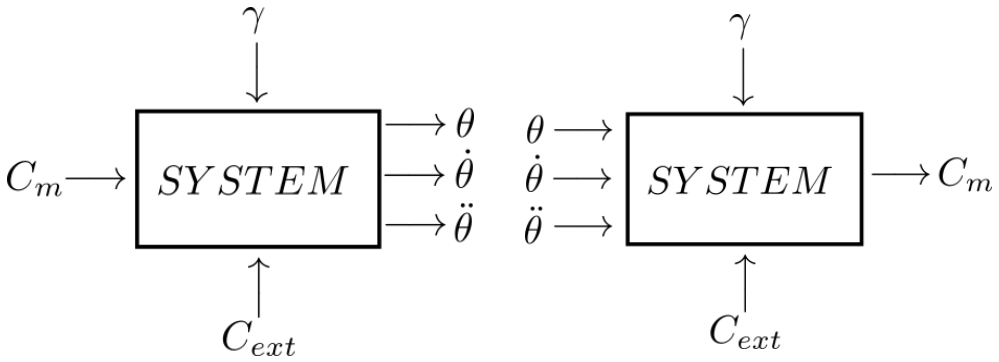

(a) Forward dynamics problem (b) Inverse dynamics problem

Figure 2.1: Forward and inverse dynamic problems

variables $q(t)$, $\dot{q}(t)$, ..., solve for the motor effort that caused such behavior.

2.2 Modeling of fundamental components

Many different architectures for compliant actuators have been proposed in the literature, but in the end they all derive from a different ordering and/or configuration of the same components in the power transmission chain.

2.2.1 Motor

Since this work is specifically targeted at industrial applications, motors and their power electronics driver are considered as an unicum. Therefore, motors will be modeled as pure torque sources (since the electrical dynamics is "hidden" by the motor drivers themselves) applied on an inertial element modeling the rotor's inertia. We will also assume of being able to control the motor torque relying on the closed-loop current/torque controller present in all motor drivers:

$$J_m\ddot{\theta}_m = C_m - b_m\dot{\theta}_m \tag{2.1}$$

In order to model energy dissipation, we will also take into consideration viscous friction b_m. For a more accurate modeling, also static friction should be considered, at least at motor side. This is particularly important when designing models for closed-loop control simulation, since phenomena such as stick-slip cannot be simulated with just pure viscous friction, and can have serious impact on real life closed-loop performance. Static friction is not proportional to relative velocity, as viscous friction, but is always present

whenever the motor moves. A discussion on accurate friction modeling and compensation strategies can be found in [27].

2.2.2 Transmission

A mechanical reduction is always needed in real applications. Planetary gearboxes, cycloidal gearboxes, or mechanically equivalent ones like Harmonic Drives, allow to obtain higher reduction ratios reducing components inertia, and at the same time offer the possibility to be employed in different configurations, including differential ones. In this work we will consider Harmonic Drives, modeled as "three-port" elements: three inertial elements, modeling the inertias of the Circular Spline (CS), Flexible Spline (FS) and Wave Generator (WG), tied together by the kinematic constraint (parametrized by i, the ratio provided by the manufacturer):

$$i\dot{\theta}_{FS} + \dot{\theta}_{WG} = (i+1)\,\dot{\theta}_{CS} \tag{2.2}$$

and power conservation, that leads to:

$$\begin{cases} \tau_{CS} = (i+1)\,\tau_{WG} \\ \tau_{FS} = -i\tau_{WG} \end{cases} \tag{2.3}$$

In addition to Equation 2.2 and 2.3, also inertial effects related to J_{WG}, J_{CS} and J_{FS} need to be considered.

2.2.3 Elastic elements

Compliant elements are fundamental components in elastic actuator. They are typically modeled as pure elasticities imposing just a linear relationship between displacement and force:

$$F = k \cdot (x - x_{eq})$$

Where $\Delta x = (x - x_{eq})$ is the displacement with respect to the spring's equilibrium position. The effect of equilibrium position can usually be neglected while modeling SEAs, but is an important aspect while designing PEAs.

In real applications such components are rarely implemented with linear or rotational springs and even if they were, the effect of nonlinearities of the torque-displacement characteristic could negatively affect the torque measurement reliability. Other effects that could be taken into consideration during modeling include:

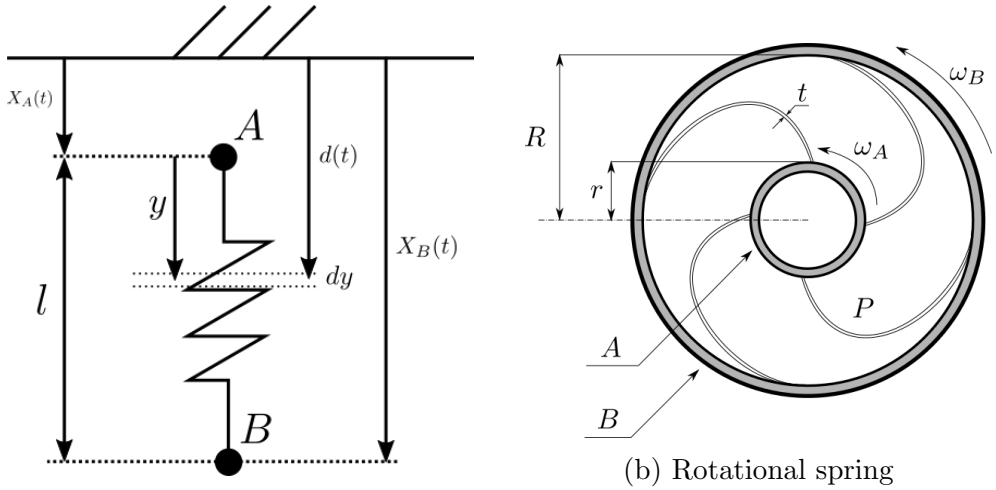

(a) Linear spring

(b) Rotational spring

Figure 2.2: Linear and rotational spring models

1. Nonlinearity of the torque/displacement relation
2. Linear or nonlinear damping
3. Non uniform or non negligible mass/inertia of the spring

In particular, the non negligible mass distribution of the spring will be considered in the following. This might seem non necessary, but since the trend and overall design criteria is to reduce the moving intertias in a robotic actuator, as a consequence the mass distribution of the spring becomes more and more non-negligible with respect to the masses/inertias of the surrounding components.

Linear Spring

Consider the spring in Figure 2.2a whose interface points, A and B, are located at positions $x_A(t)$ and $x_B(t)$ with respect to ground. Define y as the distance of a material point of length dy and mass dm with respect to A. If we define d as the position of the element dy with respect to ground it follows:

$$d(t) = x_A(t) + (x_B(t) - x_A(t))\,\frac{y}{l} \tag{2.4}$$

with $0 \leq y \leq l$. Moreover, if we define m_s as the mass of the spring, we have that:

$$dm = dy\frac{m_s}{l}$$

The infinitesimal kinetic energy of element dy is:

$$dT_s = \frac{1}{2} dm \, \dot{d}^2$$

And therefore the total kinetic energy of the spring is:

$$\begin{aligned}
T_s &= \int_{m_s} \frac{1}{2} \dot{d}^2 dm \\
&= \frac{1}{2} \int_0^l \left[\dot{x}_A + (\dot{x}_B - \dot{x}_A) \frac{y}{l} \right]^2 \frac{m_s}{l} dy \\
&= \frac{m_s}{2l} \left(\dot{x}_A^2 l + \frac{(\dot{x}_B - \dot{x}_A)^2}{l^2} \frac{l^3}{3} + \frac{2\dot{x}_A (\dot{x}_B - \dot{x}_A)}{l} \frac{l^2}{2} \right) \\
&= \frac{m_s \dot{x}_A^2}{2} + \frac{m_s \dot{x}_B^2}{6} + \frac{m_s \dot{x}_A^2}{6} - \frac{\dot{x}_A \dot{x}_B m_s}{3} + \frac{\dot{x}_A \dot{x}_B m_s}{2} - \frac{m_s \dot{x}_A^2}{2} \\
&= \frac{m_s \dot{x}_B^2}{6} + \frac{m_s \dot{x}_A^2}{6} + \frac{\dot{x}_A \dot{x}_B m_s}{6}
\end{aligned}$$

Rotational Spring

If we take Equation 2.4 and differentiate with respect to time we see that, by employing this model, we're actually making the hypothesis of a linear distribution of intermediate velocities from $\dot{x}_A$ and $\dot{x}_B$. We can employ a similar argument in analyzing the rotational spring case. Given a spring length l, the inner and outer radii r, R, the spring mass m_s, we define the linear density:

$$\rho = \frac{m_s}{l}$$

Supposing that the inner and outer flanges' velocities are, respectively, ω_1 and ω_2, and that the velocity at a generic point P on the spiral can be expressed as a function of h, with $0 \leq h \leq l$, as:

$$V_p(h) = w_1 r + \frac{w_2 R - w_1 r}{l} h \Longrightarrow \begin{cases} V_p(h=0) = \omega_1 r \\ V_p(h=L) = \omega_2 R \end{cases}$$

we can define the total kinetic energy of the spring as:

$$T_s = \frac{1}{2} \int_{m_s} V_p^2 dm = \frac{1}{2} \int_0^l V_p^2(h) \rho dh$$

Expanding, we obtain:

$$\begin{aligned} T_s &= \frac{\rho}{2}\int_0^l \left(\omega_1^2 r^2 + \frac{(\omega_2 R - \omega_1 r)^2 l^2}{L^2} + 2\frac{\omega_1 r(\omega_2 R - \omega_1 r) l}{L}\right) dh \\ &= \frac{\rho\omega_1^2 r^2 l}{2} + \frac{\rho l(\omega_2 R - \omega_1 r)^2}{6} + \frac{\rho\omega_1 r l(\omega_2 R - \omega_1 r)}{2} \\ &= \dots \\ &= \frac{m_s r^2}{6}\omega_1^2 + \frac{m_s R^2}{6}\omega_2^2 + \frac{r R m_s}{6}\omega_1\omega_2 \end{aligned}$$

That can be expressed in matrix form as the quadratic form:

$$T_s = \frac{1}{2}\begin{bmatrix}\omega_1 & \omega_2\end{bmatrix}\begin{bmatrix}\frac{m_s r^2}{3} & \frac{r R m_s}{6} \\ \frac{r R m_s}{6} & \frac{m_s R^2}{3}\end{bmatrix}\begin{bmatrix}\omega_1 \\ \omega_2\end{bmatrix}$$

2.2.4 Load

A pure visco-inertial load subject to an external torque and a motion torque will be considered:

$$J_l\ddot{\theta}_l = C_{mot} + C_{ext} - b_l\dot{\theta}_l \tag{2.5}$$

where C_{mot} is the motion torque coming from the transmission (if present) or directly from the motor itself. The viscous friction coefficient b_l is considered constant, whereas if the modeling concerned a Variable Damping Actuator this parameter would be time varying, possibly determined at runtime by the control algorithms. The external torque C_{ext} represents any additional torque acting on the output of the actuator, such as efforts due to interaction with the environment, contact, inertial forces due to off-axis masses (for example, the weight of a robot link).

2.3 Direct dynamic equation derivation: Lagrangian approach

Lagrangian approach with lumped parameters will be used as starting point of the procedure to develop the necessary dynamic equations, consisting of the following steps:

- A suitable set of physical parameters will be defined. It's important to specify the exact physical meaning of each parameter in order to be able to gather the necessary data from datasheets, measurements or experimental procedures.

- A suitable set of the most relevant kinematic quantities x_1, x_2,..., x_n will be defined. It's important to notice that this set is not necessarily the minimum set of variables to be defined as generalized Lagrangian coordinates.
- The energy functions T, U, R will be derived
- Kinematic constraints will be employed to reduce the set of motion variables to the minimum set of required Lagrangian coordinates q_1, q_2,..., q_n.
- The energy functions will be rewritten employing only the generalized Lagrangian coordinates and their derivatives.
- The vector of the generalized external non-conservative forces/torques will be derived employing the virtual work principle

$$\delta W^{nc} = \sum f^{nc} \cdot \delta x_i = \sum Q_i \cdot \delta q_i \tag{2.6}$$

- Lagrange's equations

$$\frac{d}{dt}\left(\frac{\partial T(\dot{q})}{\partial \dot{q}}\right) + \frac{\partial U(q)}{\partial q} + \frac{\partial R(\dot{q})}{\partial \dot{q}} = Q(t) \tag{2.7}$$

  can now be derived.
- The obtained equations will be rearranged in the form

$$M\ddot{q}(t) + F\dot{q}(t) + Kq(t) = E \cdot Q(t) \tag{2.8}$$

- Defining the state vector

$$x(t) = \begin{bmatrix} q(t) \\ \dot{q}(t) \end{bmatrix} \tag{2.9}$$

  and the input vector:

$$u(t) = \begin{bmatrix} Q(t) \end{bmatrix} \tag{2.10}$$

  we will transform Eq. (2.8) into state-space form:

$$\dot{x}(t) = Ax(t) + Bu(t) \tag{2.11}$$

  where:

$$A = \begin{bmatrix} 0_{2x2} & I_2 \\ -M^{-1}K & -M^{-1}F \end{bmatrix} \tag{2.12}$$

$$B = \begin{bmatrix} 0_{2x2} \\ M^{-1}E \end{bmatrix} \tag{2.13}$$

By defining a suitable output vector y the output equation will be written as:

$$y(t) = Cx(t) + Du(t) \tag{2.14}$$

with properly chosen matrices C and D.

- From the State-Space representation we will derive all the relevant transfer functions:

$$\left[G_{ij}(s)\right] = C(sI) - A)^{-1}B + D = \left(\frac{y_i}{u_j}\right)(s) \tag{2.15}$$

Equation 2.8 or its state-space counterpart Equation 2.11 and Equation 2.14 can be directly integrated in time, thus solving the direct problem.

Equation 2.8 is also the starting point for the solution of the inverse problem, as will be further discussed in the following.

The transfer functions obtained in Equation 2.15 can be employed to directly analyze the fundamental frequency responses of the mechanism, obtain resonant frequencies and study how resonant frequencies are affected by physical parameters.

2.4 Inverse dynamic solution for 1-DOF and 2-DOF systems

The mechanisms that will be considered in the following will be either 1-DOF or 2-DOF systems, subject to 2 external efforts: Γ_1, representing the motor effort, and Γ_2, representing the external effort, respectively.

To solve the direct problem we can follow the generalized procedure outlined in Section 2.3, independently from the order of the system. The solution of the inverse problem, on the contrary, is heavily dependent on the number of DOFs.

1-DOF systems

Labeling the DOF q, Equation 2.8 can be written as:

$$m\ddot{q}_1 + c\dot{q}_1 + kq_1 = e_1\Gamma_1 + e_2\Gamma_2 \tag{2.16}$$

Solution of the inverse dynamics problem is straightforward for 1-DOF systems represented by Equation 2.16. It follows from Equation 2.16 that:

$$\Gamma_1 = \frac{m\ddot{q} + c\dot{q} + kq - e_2\Gamma_2}{e_1} \tag{2.17}$$

With Equation 2.17, given the system's trajectory q_1,$\dot{q}_1$,$\ddot{q}_1$ and the external effort Γ_2 we can directly obtain Γ_1.

2-DOF systems

We label the DOFs q_1 and q_2. We also make the assumption that the motor effort Γ_1 acts only on the degree of freedom q_1 and that the external effort Γ_2 acts only on the degree of freedom q_2. Without loss of generality, Equation 2.8 can be written as:

$$\begin{cases} m_{11}\ddot{q}_1 + m_{12}\ddot{q}_2 + c_{11}\dot{q}_1 + c_{12}\dot{q}_2 + k_{11}q_1 + k_{12}q_2 + & = e_{11}\Gamma_1 \\ m_{21}\ddot{q}_1 + m_{22}\ddot{q}_2 + c_{21}\dot{q}_1 + c_{22}\dot{q}_2 + k_{21}q_1 + k_{22}q_2 + & = e_{22}\Gamma_2 \end{cases} \tag{2.18}$$

In this situation the solution is somewhat more involved, since we have 2 DOF but only one is imposed by the problem.

If we define:

$$u' = e_{22}\Gamma_2 - m_{22}\ddot{q}_2 - c_{22}\dot{q}_2 - k_{22}q_2 \tag{2.19}$$

which is a completely known signal, we can rewrite the second equation of Equation 2.18 as:

$$m_{21}\ddot{q}_1 + c_{21}\dot{q}_1 + k_{21}q_1 = u' \tag{2.20}$$

Then we distinguish three cases:

1. If $m_{21} \neq 0$ then, supposing the polynomial

   $$P(\lambda) = m_{21}\lambda^2 + c_{21}\lambda + k_{21}$$

   has roots with negative real part (or, in other words, if m_{21}, c_{21}, k_{21} are of the same sign) then Equation 2.20 can be integrated in time with initial condition $q_{1,0}$, $\dot{q}_{1,0}$ yielding the time evolution of q_1, $\dot{q}_1$ and $\ddot{q}_1$:

   $$\ddot{q}_1 = -m_{21}^{-1}c_{21}\dot{q}_1 - m_{21}^{-1}k_{21}q_1 + m_{21}^{-1}u' \Longrightarrow \int dt \Longrightarrow \begin{cases} q_1(t) \\ \dot{q}_1(t) \\ \ddot{q}_1(t) \end{cases}$$

   Finally the inverse problem can be solved by rewriting the first equation of 2.18:

   $$\Gamma_1 = \frac{m_{11}\ddot{q}_1 + m_{12}\ddot{q}_2 + c_{11}\dot{q}_1 + c_{12}\dot{q}_2 + k_{11}q_1 + k_{12}q_2}{e_{11}} \tag{2.21}$$

   where the right hand side is completely known.

2. If $m_{21} = 0$ and $c_{21} \neq 0$ then supposing the polynomial

$$P(\lambda) = c_{21}\lambda + k_{21}$$

is stable, i.e. $\frac{k_{21}}{c_{21}} > 0$ then Equation 2.20 can be integrated in time with initial condition $q_{1,0}$ yielding the time evolution of q_1 and $\dot{q}_1$:

$$\dot{q}_1 = -c_{21}^{-1}k_{21}q_1 + c_{21}^{-1}u' \Longrightarrow \int dt \Longrightarrow \begin{cases} q_1(t) \\ \dot{q}_1(t) \end{cases}$$

After obtaining $\ddot{q}_1$ either by numerical differentiation or by taking the analytic derivative (which requires the knowledge of $\dot{u}'$ and, therefore, of $\dot{\Gamma}_2$ and $\dddot{q}_2$):

$$\ddot{q}_1 = -c_{21}^{-1}k_{21}\dot{q}_1 + c_{21}^{-1}\dot{u}'$$

the inverse problem can again be solved by applying Equation 2.21.

3. If $m_{21} = 0$ and $c_{21} = 0$ then $q1$ can be algebraically obtained, without any analytical integration:

$$q_1 = \frac{u'}{k_{21}} \tag{2.22}$$

We can then obtain $\dot{q}_1$ and $\ddot{q}_1$ by numerical or analytic differentiation:

$$\dot{q}_1 = \frac{\dot{u}'}{k_{21}} \qquad \ddot{q}_1 = \frac{\ddot{u}'}{k_{21}}$$

provided we know $\dot{\Gamma}_2$, $\ddot{\Gamma}_2$, $\dddot{q}_2$,$q_2^{(4)}$. Finally, we have all the elements to solve the inverse problem using Equation 2.21.

2.5 Rigid Actuator dynamic modeling

We develop the dynamic equations for RA under the assumption of employing a Harmonic Drive as speed reducer, in the configuration having the Wave Generator connected to the input shaft, the Circular Spline Blocked and the Flexible Spline connected to the output shaft. No compliance is present in the mechanism therefore no additional inertia needs to be considered. We define the following parameters:

- J_m, representing the total inertia before the reduction. With this parameter we take into account the motor rotor inertia, the Wave Generator inertia and the moment of inertia of any part linking the two.

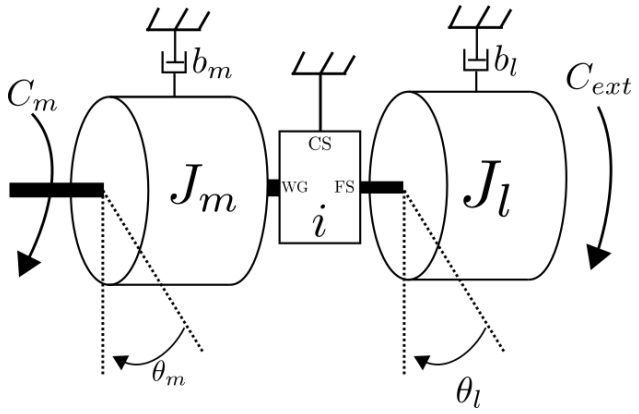

Figure 2.3: Rigid Actuator diagram

- J_l, representing the total inertia after the reduction, comprising of the Flexible Spline's inertia, the output shaft's inertia, any additional inertial load and the moment of inertia of any mechanical part in between.
- b_m, b_l, representing viscous friction at, respectively, motor and load side.
- θ_m, representing the motion variable of the inertial element J_m, i.e. the angular position of the input shaft (that coincides with the angular position of the Wave Generator).
- θ_l, representing the motion variable of the inertial element J_l, i.e. the angular position of the output shaft (that coincides with the angular position of the Flexible Spline).
- C_m representing the electro-mechanical torque produced by the motor windings. This is typically the input control variable.
- C_{ext} representing any additional torque acting on the load that is not already comprised in the inertial torque acting on J_l. This is typically an input variable that is not controllable, i.e. it can be considered as a disturbance.

RA Lagrangian analysis

We begin by defining the energy functions. The total kinetic energy can be expressed as:

$$T = \frac{1}{2} J_m \dot{\theta}_m^2 + \frac{1}{2} J_l \dot{\theta}_l^2 \tag{2.23}$$

The total potential energy is:

$$U = 0 \tag{2.24}$$

since there isn't any energy-storing component in the mechanism. The Rayleigh dissipation function is:

$$R = \frac{1}{2} b_m \dot{\theta}_m^2 + \frac{1}{2} b_l \dot{\theta}_l^2 \tag{2.25}$$

The system has one degree of freedom, therefore we can select either θ_m or θ_l as generalized coordinates. For example, we select θ_l and, by imposing the kinematic constraint due to the Harmonic Drive we have:

$$\theta_m = -i\theta_l \tag{2.26}$$

we can therefore rewrite T and R as:

$$T = \left(\frac{1}{2} J_m i^2 + \frac{1}{2} J_l \right) \dot{\theta}_l^2 \tag{2.27}$$

$$R = \left(\frac{1}{2} b_m i^2 + \frac{1}{2} b_l \right) \dot{\theta}_l^2 \tag{2.28}$$

We can then derive Lagrange's equations from Equation 2.7 where:

$$\frac{\partial T}{\partial \dot{\theta}_l} = \left(J_m i^2 + J_l \right) \dot{\theta}_l \Rightarrow \frac{d}{dt} \left(\frac{\partial T}{\partial \dot{\theta}_l} \right) = \left(J_m i^2 + J_l \right) \ddot{\theta}_l \tag{2.29}$$

$$\frac{\partial U}{\partial \theta_l} = 0 \tag{2.30}$$

$$\frac{\partial R}{\partial \dot{\theta}_l} = \left(b_m i^2 + b_l \right) \dot{\theta}_l \tag{2.31}$$

From Virtual Work Principle we get:

$$\delta W = C_m \delta\theta_m + C_{ext} \delta\theta_l = \left(C_{ext} - iC_m \right) \delta\theta_l \tag{2.32}$$

Finally, using Equations from 2.29 to 2.32 we can express the dynamic equation in the form of Equation 2.8 defining:

$$M = \left[J_m i^2 + J_l \right] \tag{2.33}$$

$$F = \left[b_m i^2 + b_l \right] \tag{2.34}$$

$$K = 0 \tag{2.35}$$

$$E = \begin{bmatrix} -i & 1 \end{bmatrix} \tag{2.36}$$

With:

$$q = \left[\theta_l \right] \tag{2.37}$$

And:

$$Q = \begin{bmatrix} C_m \\ C_{ext} \end{bmatrix} \tag{2.38}$$

RA Inverse dynamic solution

Equation 2.8 for RA can be easily inverted to solve the inverse dynamic problem. Such equation reads as:

$$\left(J_m i^2 + J_l\right) \ddot{\theta}_l + \left(b_m i^2 + b_l\right) \dot{\theta}_l = C_{ext} - i C_m \tag{2.39}$$

From which:

$$C_m = \frac{C_{ext} - \left(J_m i^2 + J_l\right) \ddot{\theta}_l - \left(b_m i^2 + b_l\right) \dot{\theta}_l}{i} \tag{2.40}$$

With Equation 2.40, once the external torque signal $C_{ext}(t)$ is known and the desired output behavior is specified, by means of the signals $\dot{\theta}_l(t)$ and $\ddot{\theta}_l(t)$, the required motor torque $C_m(t)$ can immediately be computed.

2.6 Parallel Elastic Actuator dynamic modeling

We develop the dynamic equations for PEA under the assumption of employing a Harmonic Drive as speed reducer, in the configuration having the Wave Generator connected to the input shaft, the Circular Spline Blocked and the Flexible Spline connected to the output shaft. Compliance is present in the mechanism in parallel to the transmission with respect to the load, thus connecting the ground and the load itself. We define the following parameters:

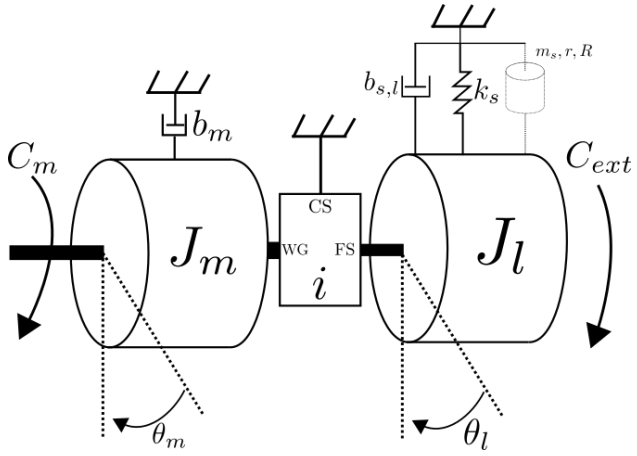

Figure 2.4: Parallel Elastic Actuator diagram

- J_m, representing the total inertia before the reduction. With this parameter we take into account the motor rotor inertia, the Wave Generator inertia and the moment of inertia of any part linking the two.

- J_l, representing the total inertia after the reduction, comprising of the Flexible Spline's inertia, the output shaft's inertia, any additional inertial load and the moment of inertia of any mechanical part in between.

- b_m, $b_{s,l}$: the first representing viscous friction at motor side and the second representing viscous friction both at the load and due to the spring.

- k_s, representing the spring constant of the elastic element

- θ_m, representing the motion variable of the inertial element J_m, i.e. the angular position of the input shaft (that coincides with the angular position of the Wave Generator).

- θ_l, representing the motion variable of the inertial element J_l, i.e. the angular position of the output shaft (that coincides with the angular position of the Flexible Spline). In PEAs, θ_l also represents the deflection of the elastic element with respect to its zero non-deformed position.

- C_m representing the electro-mechanical torque produced by the motor windings. This is typically the input control variable.

- C_{ext} representing any additional torque acting on the load that is not already comprised in the inertial torque acting on J_l. This is typically an input variable that is not controllable, i.e. it can be considered as a disturbance.

PEA Lagrangian analysis

We begin by defining the energy functions. The total kinetic energy can be expressed as:

$$T = \frac{1}{2} J_m \dot{\theta}_m^2 + \frac{1}{2} J_l \dot{\theta}_l^2 \tag{2.41}$$

The total potential energy is:

$$U = \frac{1}{2} k_s \theta_l^2 \tag{2.42}$$

The Rayleigh dissipation function is:

$$R = \frac{1}{2} b_m \dot{\theta}_m^2 + \frac{1}{2} b_{s,l} \dot{\theta}_l^2 \tag{2.43}$$

The system has one degree of freedom, therefore we can select either θ_m or θ_l as generalized coordinates. For example, we select θ_l and, by imposing the kinematic constraint due to the Harmonic Drive we have:

$$\theta_m = -i\theta_l \tag{2.44}$$

we can therefore rewrite T, U, R as:

$$T = \left(\frac{1}{2} J_m i^2 + \frac{1}{2} J_l \right) \dot{\theta}_l^2 \tag{2.45}$$

$$U = \frac{1}{2} k_s \theta_l^2 \tag{2.46}$$

$$R = \left(\frac{1}{2} b_m i^2 + \frac{1}{2} b_{s,l} \right) \dot{\theta}_l^2 \tag{2.47}$$

We can then derive Lagrange's equations from 2.7 where:

$$\frac{\partial T}{\partial \dot{\theta}_l} = \left(J_m i^2 + J_l \right) \dot{\theta}_l \Rightarrow \frac{d}{dt} \left(\frac{\partial T}{\partial \dot{\theta}_l} \right) = \left(J_m i^2 + J_l \right) \ddot{\theta}_l \tag{2.48}$$

$$\frac{\partial U}{\partial \theta_l} = k_s \theta_l \tag{2.49}$$

$$\frac{\partial R}{\partial \dot{\theta}_l} = \left(b_m i^2 + b_{s,l} \right) \dot{\theta}_l \tag{2.50}$$

From Virtual Work Principle we get:

$$\delta W = C_m \delta\theta_m + C_{ext} \delta\theta_l = \left(C_{ext} - i C_m \right) \delta\theta_l \tag{2.51}$$

Finally, using from Equation 2.29 to 2.32 we can express the dynamic equation in the form of Equation 2.8 defining:

$$M = \begin{bmatrix} J_m i^2 + J_l \end{bmatrix} \tag{2.52}$$

$$F = \begin{bmatrix} b_m i^2 + b_{s,l} \end{bmatrix} \tag{2.53}$$

$$K = \begin{bmatrix} k_s \end{bmatrix} \tag{2.54}$$

$$E = \begin{bmatrix} -i & 1 \end{bmatrix} \tag{2.55}$$

With:

$$q = \begin{bmatrix} \theta_l \end{bmatrix} \tag{2.56}$$

And:

$$Q = \begin{bmatrix} C_m \\ C_{ext} \end{bmatrix} \tag{2.57}$$

PEA Inverse dynamic solution

Equation 2.8 for PEA can be easily inverted to solve the inverse dynamic problem. Such equation reads as:

$$\left(J_m i^2 + J_l\right) \ddot{\theta}_l + \left(b_m i^2 + b_{s,l}\right) \dot{\theta}_l + k_s \theta_l = C_{ext} - i C_m \tag{2.58}$$

From which:

$$C_m = \frac{C_{ext} - \left(J_m i^2 + J_l\right) \ddot{\theta}_l - \left(b_m i^2 + b_{s,l}\right) \dot{\theta}_l - k_s \theta_l}{i} \tag{2.59}$$

With Equation 2.59, once the external torque signal $C_{ext}(t)$ is known and the desired output behavior is specified, by means of the signals θ_l, $\dot{\theta}_l(t)$ and $\ddot{\theta}_l(t)$, the required motor torque $C_m(t)$ can immediately be computed.

2.7 Series Elastic Actuator dynamic modeling

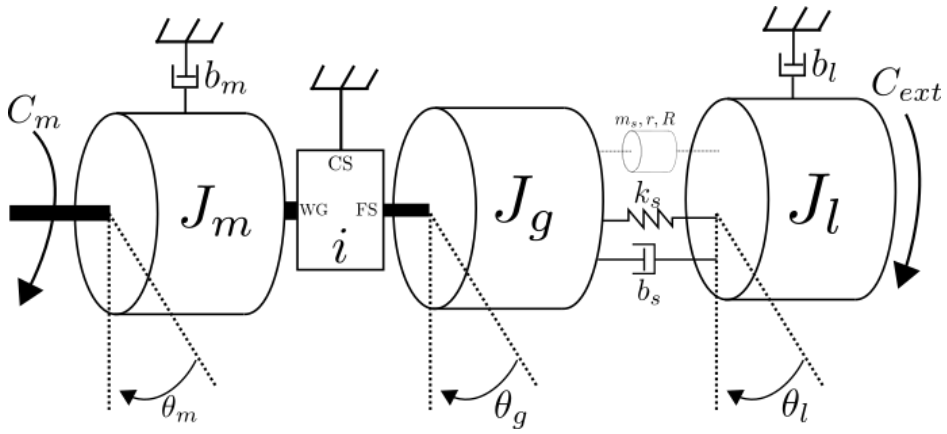

Figure 2.5: Series Elastic Actuator diagram

We develop the dynamic equations for SEAs under the assumption of employing a Harmonic Drive as speed reducer, in the configuration having the Circular Spline blocked, the input shaft connected to the Wave Generator and the outer spring ring connected to the Flexible Spline. The inner spring ring is connected to the output shaft and the load.

In SEAs both flanges of the spring can rotate, therefore we define the spring kinetic energy as:

$$T_s = \frac{m_s r^2}{6} \dot{\theta}_l^2 + \frac{m_s R^2}{6} \dot{\theta}_g^2 + \frac{r R m_s}{6} \dot{\theta}_l \dot{\theta}_g \tag{2.60}$$

We define the following parameters:

- J_m, representing the total inertia before the reduction. With this parameter we take into account the motor rotor inertia, the Wave Generator inertia and the moment of inertia of any part linking the two.
- J_g, representing the Flexible Spline inertia, the spring's outer ring inertia and the moment of inertia of any part linking the two.
- J_l, representing the output shaft's inertia, any additional inertial load and the moment of inertia of any part in between.
- b_m, b_l, b_s, representing viscous friction at, respectively, motor and load side and inside the spring.
- k_s, representing the spring constant of the spring element.
- θ_m, representing the motion variable of the inertial element J_m, i.e. the angular position of the input shaft (that coincides with the angular position of the Wave Generator).
- θ_g, representing the motion variable of the inertial element J_g, i.e. the angular position of the spring's outer ring with respect to ground (that coincides with the angular position of the Flexible Spline).
- θ_l, representing the motion variable of the inertial element J_l, i.e. the angular position of the inner spring ring and of the output shaft.

SEA Lagrangian Analysis

We begin by defining the energy functions. The total kinetic energy can be expressed as:

$$T = \frac{1}{2}J_m\dot{\theta}_m^2 + \frac{1}{2}J_l\dot{\theta}_l^2 + \frac{1}{2}J_g\dot{\theta}_g^2 + T_s \tag{2.61}$$

The total potential energy is:

$$U = \frac{1}{2}k_s\theta_s^2 \tag{2.62}$$

The Rayleigh dissipation function is:

$$R = \frac{1}{2}b_m\dot{\theta}_m^2 + \frac{1}{2}b_l\dot{\theta}_l^2 + \frac{1}{2}b_s\dot{\theta}_s^2 \tag{2.63}$$

The system has two degrees of freedom, therefore we select as generalized coordinates the angles θ_m and θ_l and, by imposing the kinematic constraints:

$$\theta_g = -\frac{\theta_m}{i} \tag{2.64}$$

$$\theta_s = \theta_l - \theta_g = \theta_l + \frac{\theta_m}{i} \tag{2.65}$$

we can rewrite T, U, R as:

$$T = \left(\frac{m_s r^2}{6} + \frac{J_l}{2}\right)\dot{\theta}_l^2 - \left(\frac{J_m i^2 + J_g}{2i^2} + \frac{R^2 m_s}{6i^2}\right)\dot{\theta}_m^2 + \frac{R r m_s}{6i}\dot{\theta}_m\dot{\theta}_l \tag{2.66}$$

$$U = \frac{k_s}{2}\theta_l^2 + \frac{k_s}{2i^2}\theta_m^2 + \frac{k_s}{i}\theta_l\theta_m \tag{2.67}$$

$$R = \left(\frac{b_l + b_s}{2}\right)\dot{\theta}_l^2 + \left(\frac{b_m i^2 + b_s}{2i^2}\right)\dot{\theta}_m^2 + \frac{b_s}{i}\dot{\theta}_m\dot{\theta}_l \tag{2.68}$$

We can then derive the Lagrange's equations:

$$\frac{d}{dt}\left(\frac{\partial T}{\partial \dot{q}}\right) + \frac{\partial U}{\partial q} + \frac{\partial R}{\partial \dot{q}} = Q \tag{2.69}$$

Where:

$$\frac{\partial T}{\partial \dot{\theta}_m} = \left(\frac{m_s R^2 + 3J_m i^2 + 3J_g}{3i^2}\right)\dot{\theta}_m - \frac{R r m_s}{6i}\dot{\theta}_l \tag{2.70}$$

$$\frac{\partial T}{\partial \dot{\theta}_l} = -\frac{R r m_s}{6i}\dot{\theta}_m + \left(\frac{m_s r^2}{3} + J_l\right)\dot{\theta}_l \tag{2.71}$$

$$\frac{d}{dt}\left(\frac{\partial T}{\partial \dot{\theta}_m}\right) = \left(\frac{m_s R^2 + 3J_m i^2 + 3J_g}{3i^2}\right)\ddot{\theta}_m - \frac{R r m_s}{6i}\ddot{\theta}_l \tag{2.72}$$

$$\frac{d}{dt}\left(\frac{\partial T}{\partial \dot{\theta}_l}\right) = -\frac{R r m_s}{6i}\ddot{\theta}_m + \left(\frac{m_s r^2}{3} + J_l\right)\ddot{\theta}_l \tag{2.73}$$

$$\frac{\partial U}{\partial \theta_m} = \frac{k_s}{i^2}\theta_m + \frac{k_s}{i}\theta_l \tag{2.74}$$

$$\frac{\partial U}{\partial \theta_l} = \frac{k_s}{i}\theta_m + k_s\theta_l \tag{2.75}$$

$$\frac{\partial R}{\partial \dot{\theta}_m} = \left(b_m + \frac{b_s}{i^2}\right)\dot{\theta}_m + \frac{b_s}{i}\dot{\theta}_l \tag{2.76}$$

$$\frac{\partial R}{\partial \dot{\theta}_l} = \frac{b_s}{i}\dot{\theta}_m + (b_l + b_s)\,\dot{\theta}_l \tag{2.77}$$

Employing Virtual Work Principle we get:

$$\delta W = C_m \delta\theta_m + C_{ext}\delta\theta_l \Longrightarrow \begin{cases} Q_{\theta_m} = C_m \\ Q_{\theta_l} = C_{ext} \end{cases} \tag{2.78}$$

Finally, using from Equation 2.72 to Equation 2.78 we can express the dynamic equations in the form of Equation 2.8 defining the matrices:

$$M = \begin{bmatrix} J_m + \frac{m_s R^2 + 3J_g}{3i^2} & -\frac{Rrm_s}{6i} \\ -\frac{Rrm_s}{6i} & \frac{m_s r^2}{3} + J_l \end{bmatrix} \tag{2.79}$$

$$F = \begin{bmatrix} b_m + \frac{b_s}{i^2} & \frac{b_s}{i} \\ \frac{b_s}{i} & b_l + b_s \end{bmatrix} \tag{2.80}$$

$$K = \begin{bmatrix} \frac{k_s}{i^2} & \frac{k_s}{i} \\ \frac{k_s}{i} & k_s \end{bmatrix} \tag{2.81}$$

$$E = \begin{bmatrix} 1 & 0 \\ 0 & 1 \end{bmatrix} \tag{2.82}$$

With:

$$q = \begin{bmatrix} \theta_m \\ \theta_l \end{bmatrix} \tag{2.83}$$

And:

$$Q = \begin{bmatrix} C_m \\ C_{ext} \end{bmatrix} \tag{2.84}$$

SEA Inverse dynamics solution

Equation 2.8 for SEA can be inverted in two steps, as outlined in Section 2.4. For simplicity, here we will neglect friction and the inertial effects of the spring. Under these assumptions, Equation 2.8 for SEA can be written as:

$$\begin{cases} \left(J_m + \dfrac{J_g}{i^2}\right)\ddot{\theta}_m + \dfrac{k_s}{i^2}\theta_m + \dfrac{k_s}{i}\theta_l = C_m \\ J_l\ddot{\theta}_l + \dfrac{k_s}{i}\theta_m + k_s\theta_l = C_{ext} \end{cases} \tag{2.85}$$

From the second equation of 2.85 we can obtain:

$$\theta_m = \frac{i}{k_s}\left(C_{ext} - k_s\theta_l - J_l\ddot{\theta}_l\right) \tag{2.86}$$

Substituting Equation 2.86 into the first equation of 2.85 and simplifying we obtain:

$$C_m = i\left(J_m + \frac{J_g}{i^2}\right)\left(\frac{\ddot{C}_{ext} - J_l\theta_l^{(4)}}{k} - \ddot{\theta}_l\right) + \frac{C_{ext} - J_l\ddot{\theta}_l}{i} \tag{2.87}$$

With Equation 2.87, once the desired motion trajectory $\theta_l(t)$ and external torque $C_{ext}(t)$ are known, up to the fourth and second derivatives, respectively, the necessary motor torque $C_m(t)$ can be computed.

2.8 Differential Elastic Actuator dynamic modeling

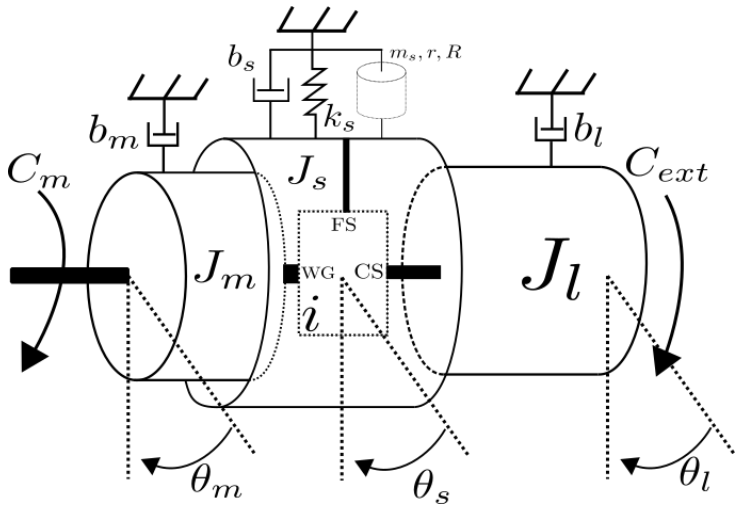

Figure 2.6: Differential elastic actuator diagram

We develop the dynamic equations for DEAs under the assumption of employing a Harmonic Drive as speed reducer, in the configuration having the Circular Spline connected to the output shaft, and therefore to the load, the input shaft connected to the Wave Generator and the Flexible Spline connected to the outer ring of the rotational spring.

In the DEA case either the inner or outer flange of the spring is connected to ground. Supposing we ground the inner flange, imposing $\omega_1 = 0$ the spring kinetic energy changes to:

$$T_s = \frac{m_s R^2}{6}\dot{\theta}_s^2 \tag{2.88}$$

We define the following parameters:

- J_m, representing the total inertia before the reduction. With this parameter we take into account the rotor inertia, the Wave Generator inertia and the moment of inertia of any part linking the two.
- J_s, representing the Flexible Spline inertia, the spring's outer ring inertia and the moment of inertia of any part linking the two.
- J_l, representing the Circular Spline Inertia, the output shaft's inertia, any additional inertial load and the moment of inertia of any part in between.
- b_m, b_s, b_l, representing viscous friction at, respectively, motor, spring and load side.
- k_s, representing the spring constant of the spring element.
- θ_m, representing the motion variable of the inertial element J_m, i.e. the angular position of the input shaft (that coincides with the angular position of the Wave Generator).
- θ_s, representing the motion variable of the inertial element J_s, i.e. the angular position of the spring's outer ring with respect to ground (that coincides with the angular position of the Flexible Spline).
- θ_l, representing the motion variable of the inertial element J_l, i.e. the angular position of the output shaft (that coincides with the angular position of the Circular Spline).

DEA Lagrangian Analysis

We can express the total kinetic energy as:

$$T = \frac{1}{2}J_m\dot{\theta}_m^2 + \frac{1}{2}J_l\dot{\theta}_l^2 + \frac{1}{2}J_s\dot{\theta}_s^2 + T_s \tag{2.89}$$

The total potential energy is:

$$U = \frac{1}{2}k_s\theta_s^2 \tag{2.90}$$

The Rayleigh dissipation function is:

$$R = \frac{1}{2}b_m\dot{\theta}_m^2 + \frac{1}{2}b_l\dot{\theta}_l^2 + \frac{1}{2}b_s\dot{\theta}_s^2 \tag{2.91}$$

We select as generalized coordinates the angles θ_m and θ_l. Therefore, by imposing the kinematic constraint enforced by the Harmonic Drive:

$$i\theta_s = (i+1)\theta_l - \theta_m \tag{2.92}$$

we are able to express T, U, R as function of only θ_m, θ_l and their derivatives:

$$T = \left(\frac{J_l}{2} + \frac{(3J_s + R^2 m_s)(i+1)^2}{6i^2}\right)\dot{\theta}_l^2 + \left(\frac{J_m}{2} + \frac{3J_s + R^2 m_s}{6i^2}\right)\dot{\theta}_m^2 + \\ - \left(\frac{(3J_s + R^2 m_s)(i+1)}{3i^2}\right)\dot{\theta}_m\dot{\theta}_l \tag{2.93}$$

$$U = \frac{k_s(i+1)^2}{2i^2}\theta_l^2 + \frac{k_s}{2i^2}\theta_m^2 - \frac{k_s(i+1)}{i^2}\theta_m\theta_l \tag{2.94}$$

$$R = \left(\frac{b_l}{2} + \frac{b_s(i+1)^2}{2i^2}\right)\dot{\theta}_l^2 + \left(\frac{b_m}{2} + \frac{b_s}{2i^2}\right)\dot{\theta}_m^2 - \frac{b_s(i+1)}{i^2}\dot{\theta}_m\dot{\theta}_l \tag{2.95}$$

We can then derive the Lagrange's equations:

$$\frac{d}{dt}\left(\frac{\partial T}{\partial \dot{q}}\right) + \frac{\partial U}{\partial q} + \frac{\partial R}{\partial \dot{q}} = Q \tag{2.96}$$

Where:

$$\frac{\partial T}{\partial \dot{\theta}_m} = \left(J_m + \frac{3J_s + R^2 m_s}{3i^2}\right)\dot{\theta}_m - \left(\frac{(3J_s + R^2 m_s)(i+1)}{3i^2}\right)\dot{\theta}_l \tag{2.97}$$

$$\frac{\partial T}{\partial \dot{\theta}_l} = -\left(\frac{(3J_s + R^2 m_s)(i+1)}{3i^2}\right)\dot{\theta}_m + \left(J_l + \frac{(3J_s + R^2 m_s)(i+1)^2}{3i^2}\right)\dot{\theta}_l \tag{2.98}$$

$$\frac{d}{dt}\left(\frac{\partial T}{\partial \dot{\theta}_m}\right) = \left(J_m + \frac{3J_s + R^2 m_s}{3i^2}\right)\ddot{\theta}_m - \left(\frac{(3J_s + R^2 m_s)(i+1)}{3i^2}\right)\ddot{\theta}_l \tag{2.99}$$

$$\frac{d}{dt}\left(\frac{\partial T}{\partial \dot{\theta}_l}\right) = -\left(\frac{(3J_s + R^2 m_s)(i+1)}{3i^2}\right)\ddot{\theta}_m + \left(J_l + \frac{(3J_s + R^2 m_s)(i+1)^2}{3i^2}\right)\ddot{\theta}_l \tag{2.100}$$

$$\frac{\partial U}{\partial \theta_m} = \frac{k_s}{i^2}\theta_m - \frac{k_s(i+1)}{i^2}\theta_l \tag{2.101}$$

$$\frac{\partial U}{\partial \theta_l} = -\frac{k_s(i+1)}{i^2}\theta_m + \frac{k_s(i+1)^2}{i^2}\theta_l \tag{2.102}$$

$$\frac{\partial R}{\partial \dot{\theta}_m} = \left(b_m + \frac{b_s}{i^2}\right)\dot{\theta}_m - \frac{b_s(i+1)}{i^2}\dot{\theta}_l \tag{2.103}$$

$$\frac{\partial R}{\partial \dot{\theta}_l} = -\left(\frac{b_s(i+1)}{i^2}\right)\dot{\theta}_m + \left(b_l + \frac{b_s(i+1)^2}{i^2}\right)\dot{\theta}_l \tag{2.104}$$

Employing Virtual Work Principle we get:

$$\delta W = C_m\delta\theta_m + C_{ext}\delta\theta_l \Longrightarrow \begin{cases} Q_{\theta_m} = C_m \\ Q_{\theta_l} = C_{ext} \end{cases} \tag{2.105}$$

Finally, using from Equation 2.99 to Equation 2.105 we can express the dynamic equations in the form of Equation 2.8 defining the matrices:

$$M = \begin{bmatrix} J_m + \frac{3J_s+R^2m_s}{3i^2} & -\frac{(i+1)(3J_s+R^2m_s)}{3i^2} \\ -\frac{(i+1)(3J_s+R^2m_s)}{3i^2} & J_l + \frac{(3J_s+R^2m_s)(i+1)^2}{3i^2} \end{bmatrix} \tag{2.106}$$

$$F = \begin{bmatrix} b_m + \frac{b_s}{i^2} & -\frac{b_s(i+1)}{i^2} \\ -\frac{b_s(i+1)}{i^2} & b_l + \frac{b_s(i+1)^2}{i^2} \end{bmatrix} \tag{2.107}$$

$$K = \begin{bmatrix} \frac{k_s}{i^2} & -\frac{k_s(i+1)}{i^2} \\ -\frac{k_s(i+1)}{i^2} & \frac{k_s(i+1)^2}{i^2} \end{bmatrix} \tag{2.108}$$

$$E = \begin{bmatrix} 1 & 0 \\ 0 & 1 \end{bmatrix} \tag{2.109}$$

With:

$$q = \begin{bmatrix} \theta_m \\ \theta_l \end{bmatrix} \tag{2.110}$$

And:

$$Q = \begin{bmatrix} C_m \\ C_{ext} \end{bmatrix} \tag{2.111}$$

DEA Inverse dynamics solution

Equation 2.8 for DEA can be inverted using the procedure outlined in Section 2.4. For simplicity, here we will neglect the inertial effects of the spring and friction. Under these assumptions, Equation 2.8 for DEA can be written as:

$$\begin{cases} \left(J_m + \frac{J_s}{i^2}\right)\ddot{\theta}_m - \frac{(i+1)\,J_s}{i^2}\ddot{\theta}_l + \frac{k_s}{i^2}\theta_m - \frac{(i+1)\,k_s}{i^2}\theta_l = C_m \\ -\frac{(i+1)\,J_s}{i^2}\ddot{\theta}_m + \left(J_l + \left(\frac{i+1}{i}\right)^2 J_s\right)\ddot{\theta}_l - \frac{(i+1)\,k_s}{i^2}\theta_m + k_s\left(\frac{i+1}{i}\right)^2\theta_l = C_{ext} \end{cases} \tag{2.112}$$

We notice immediately that in the second equation of 2.112 we have both θ_m and its second derivative. A full analytic solution would then require the

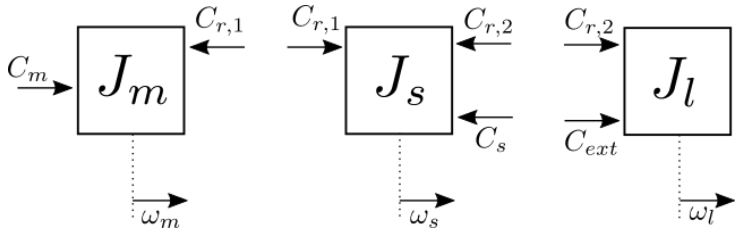

Figure 2.7: Free Body Diagram for DEA

solution of a differential equation in order to obtain θ_m and its derivatives to be plugged in the first equation of 2.112. To proceed with an analytic solution as for the SEA case, a simplification needs to be introduced.

In order to follow the usual procedure we would need to algebraically obtain θ_m from the second equation of 2.112, thus we would need to get rid of $\ddot{\theta}_m$. Employing the transmission constraint enforced by Equation 2.92 as is would not be enough since we would introduce $\ddot{\theta}_s$ in the equations. The idea is, therefore, to neglect the inertial effects produced by J_s, which is a reasonable assumption under the hypothesis of negligible spring acceleration.

To better understand the simplification, Figure 2.7 shows the free body diagram of the DEA, where $C_{r,1}$ and $C_{r,2}$ are internal reaction torques. The free body diagram analysis brings to the following set of equations ad dynamic equilibrium:

$$\begin{cases} C_m - C_{r,1} = J_m \dot{\omega}_m \\ C_{r,1} - C_{r,2} - C_s = J_s \dot{\omega}_s \\ C_{r,2} + C_{ext} = J_l \dot{\omega}_l \end{cases} \tag{2.113}$$

Moreover, if we focus our attention only on the spring inertial element and apply the power conservation law at static equilibrium, enforcing the kinematic constraint, we can write:

$$\begin{cases} C_{r,1} - C_s - C_{r,2} = 0 \\ C_{r,1}\omega_m - C_s\omega_s - C_{r,2}\omega_l = 0 \\ \omega_m = \omega_l\,(i+1) - \omega_s i \end{cases} \tag{2.114}$$

Solving the set of equations 2.114 with respect to C_s and $C_{r,1}$, allows us to obtain:

$$C_s \approx -\frac{i}{i+1} C_{r,2} \tag{2.115}$$

Equation 2.115, which holds exactly at static equilibrium and approximately at dynamic equilibrium, will be used as the starting point for the approximation. Since:

$$C_s = k\theta_s \tag{2.116}$$

then, applying both Equation 2.115 and Equation 2.116 we obtain:

$$\theta_s \approx -\frac{i}{k\,(i+1)} C_{r,2} \tag{2.117}$$

From dynamic equilibrium of body J_l (i.e. form third equation of Equation 2.113) we have that:

$$C_{r,2} = J_l \dot{\omega}_l - C_{ext} \tag{2.118}$$

and therefore, finally, we obtain:

$$\theta_s \approx -\frac{i}{k\,(i+1)} \left(J_l \ddot{\theta}_l - C_{ext} \right) \tag{2.119}$$

Using Equation 2.119 in the kinematic constraint 2.92 we can derive:

$$\ddot{\theta}_m = (i+1)\,\ddot{\theta}_l - i\ddot{\theta}_s \tag{2.120}$$

$$\approx (i+1)\,\ddot{\theta}_l + \frac{i^2}{k\,(i+1)} \left(J_l \theta_l^{(4)} - \ddot{C}_{ext} \right) \tag{2.121}$$

By substituting 2.121 in the second equation of 2.112 we can now algebraically solve for θ_m:

$$\theta_m = (i+1)\,\theta_l - \frac{ki^2 \left(C_{ext} - J_l \ddot{\theta}_l \right) - J_s i^2 \left(\ddot{C}_{ext} - J_l \theta_l^{(4)} \right)}{k^2\,(i+1)} \tag{2.122}$$

Substituting Equation 2.122 into the first equation of 2.112 we obtain an approximate expression for C_m:

$$C_m = \frac{J_m\,(i+1)^2 + J_l}{i+1} \ddot{\theta}_l - \frac{C_{ext}}{i+1} - \frac{J_m i^2 \left(\ddot{C}_{ext} - J_l \theta_l^{(4)} \right)}{k\,(i+1)} \tag{2.123}$$

Chapter 3

Actuator Optimization

In this chapter a procedure for the design optimization of robotic actuators is presented. First, the traditional method used to optimize power transmission chains is presented, together with some considerations on why this approach does not scale appropriately when applied to non-rigid actuators. In the following an extended optimization approach is presented, that heavily relies upon the preceding modeling phase, and in particular on the solution of the inverse dynamic problem for the selected actuator. Some commonly used merit figures used in optimization are presented and applied to some example use-cases. The results of the optimization on these use-cases in analyzed.

3.1 Introduction

Series Elastic Actuators (SEAs) have become ubiquitous in the robotics literature since their first appearance, due to their ability to passively store mechanical energy, thereby providing lower output impedance and tolerance to shocks and impacts.

Traditional stiff actuators, despite being perfectly suited for precise and repeatable positioning tasks, fail in applications in which the interaction with the external environment is either necessary, such as in rehabilitation devices where the machine is in physical contact with the patient, or desirable, such as in industrial scenarios where machine operation requires the highest level of safety and compliance to avoid damages to equipment and injuries to people.

The introduction of elastic elements on the one hand provides the additional compliance required by the tasks, but on the other hand increases the complexity of the actuator, in terms of both control law development and mechanical design. In this context, proper techniques and guidelines

for SEA design need to be devised, possibly adapting those already used for traditional stiff actuators.

In the literature, the optimal selection of actuator transmission ratio is a well know problem, for which many different approaches and objective functions have been proposed.

As an example, in [15] two decoupled performance indices are defined, one related with the motor and the other with the load characteristics and compared to assess the correct choice of the actuator for the given task. In [7] also the mechanical limits of both motor and transmission are taken into consideration. In [24] the general principle of inertia matching is conceived, which states that under given loading conditions the optimal transmission ratio is the one that balances the inertia of the motor and the load, both referred to the same shaft. Under this condition, the power provided by the motor is therefore equally distributed between motor and load.

Detailed practical procedures for the optimal selection of actuator components can be found in [8] and [25]. In [21] this principle is generalized, performing optimization under general load cases and introducing as objective function also the bandwidth of the closed-loop actuator together with energy. In [3] and [29] also the electric motor is taken into consideration, introducing in the optimization problem the power losses in both electrical and mechanical domains. In [17] the problem of the simultaneous optimization of actuator parameters, control efficiency and motion law selection, applied to a manipulator with several motors, is formulated and solved employing multi-objective genetic algorithms.

Nonetheless, the vast majority of the existing works only deal with traditional stiff actuators, which are always represented as single degree of freedom mechanical systems. In regard to the modeling of actuators with elastic transmission elements, a very concise and general discussion can be found in [14], which however is not aimed at actuator sizing, while optimization of the natural frequencies arising from the introduction of compliant elements in the power transmission is addressed in [29].

In this work, the combined effect of transmission ratio and stiffness on SEA motor requirements is investigated via a theoretical approach. A procedure is presented to help the designer in the selection of the best combination of the two parameters that minimize a certain norm function of motor torque and power.

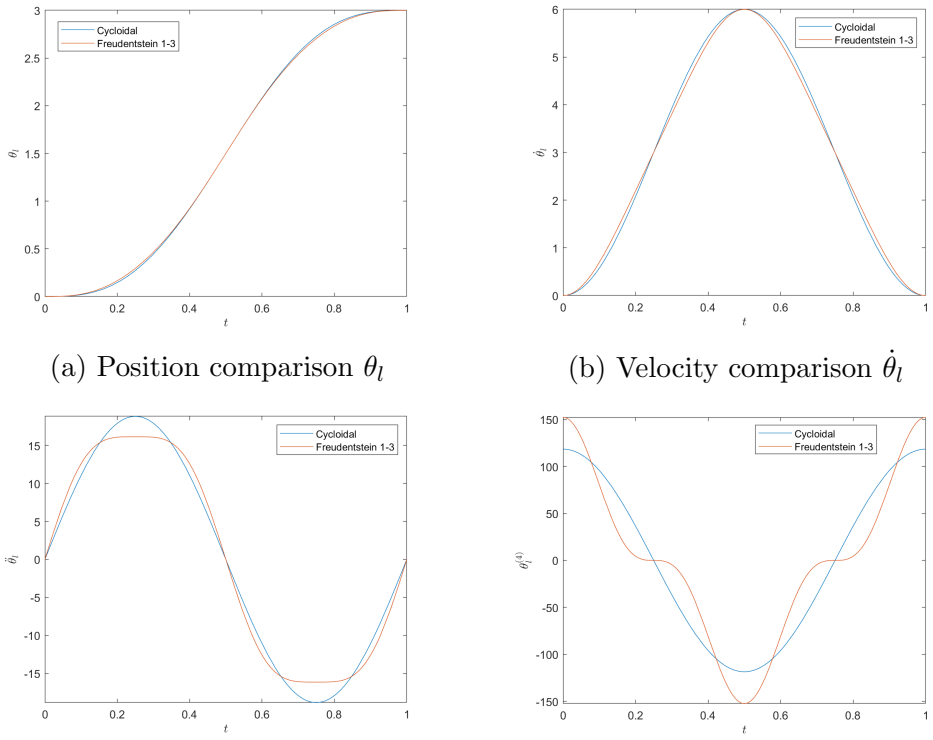

(a) Position comparison θ_l

(b) Velocity comparison $\dot{\theta}_l$

(c) Acceleration comparison $\ddot{\theta}_l$

(d) Jerk comparison $\dddot{\theta}_l$

Figure 3.1: Numerical comparison of Cycloidal and Freudenstein 1-3 trajectories and their derivatives

3.2 Traditional optimization approach

The traditional approach applied to RA presented in [15] considers a dynamic model equivalent to the one presented in Figure 2.3, neglecting viscous friction and other sources of energy losses, thus considering an ideal actuator with efficiency of 1. Therefore, it's possible to obtain the expression for the motor torque simplifying Equation 2.40:

$$C_m = \frac{C_{ext} - (J_m i^2 + J_l)\,\ddot{\theta}_l}{i} \tag{3.1}$$

The original problem consists of finding the best value of the transmission ratio i that optimizes the RMS motor torque:

$$C_{m,RMS}^2 = \frac{1}{T}\int_0^T C_m^2(t)dt \tag{3.2}$$

Therefore, by substituting and considering $C_{ext} = 0$ we obtain:

$$C_{m,RMS}^2 = \frac{1}{T}\int_0^T \frac{\left(J_m i^2 + J_l\right)^2 \ddot{\theta}_l^2(t)}{i^2} dt \tag{3.3}$$

$$= \frac{\left(J_m i^2 + J_l\right)^2}{i^2}\frac{1}{T}\int_0^T \ddot{\theta}_l^2(t)\, dt \tag{3.4}$$

$$= \frac{\left(J_m i^2 + J_l\right)^2}{i^2}\ddot{\theta}_{L,RMS}^2 \tag{3.5}$$

Deriving with respect to i we obtain:

$$\frac{dC_{m,RMS}^2}{di} = \frac{4\left(J_m i^2 + J_l\right) J_m i^3 - 2\left(J_m i^2 + J_l\right)^2 i}{i^4}\ddot{\theta}_{L,RMS}^2 \tag{3.6}$$

$$= 2\frac{J_m^2 i^4 - J_l^2}{i^3}\ddot{\theta}_{L,RMS}^2 \tag{3.7}$$

And imposing it to be equal to zero we obtain the optimal solution:

$$\frac{dC_{m,RMS}^2}{di} = 0 \Leftrightarrow J_m^2 i^4 - J_l^2 = 0 \Leftrightarrow i_{opt} = \sqrt{\frac{J_l}{J_m}} \tag{3.8}$$

In this scenario it was possible to derive an optimal value for the only design parameter available, the transmission ratio i, irrespective of the imposed motion trajectory $\theta_l(t)$. The optimal transmission ratio only depends on the inertial properties of the actuator and of the load.

3.3 Extended optimization approach

Generalizing the procedure presented in the previous section for 2-DOF actuators consists in finding the transmission parameter i and spring stiffness k that minimize a certain objective function. The most commonly used objective function is a certain p-norm of an actuator-related quantity that expresses the efficiency of the actuator itself in performing a certain task $\theta_l(t)$ under loading condition $C_{ext}(t)$ within a given period of time t_a.

The p-norm of a function is defined as:

$$\left\|F(i,k)\right\|_p = \sqrt[p]{\frac{1}{t_a}\int_0^{t_a} \left[F(i,k)\right]^p dt} \tag{3.9}$$

And therefore the optimization problem can be formalized as:

$$\begin{aligned} \min_{i,k} \quad & \left\|F(i,k)\right\|_p \\ \text{s.t.} \quad & \text{physical feasibility constraints are satisfied} \end{aligned} \tag{3.10}$$

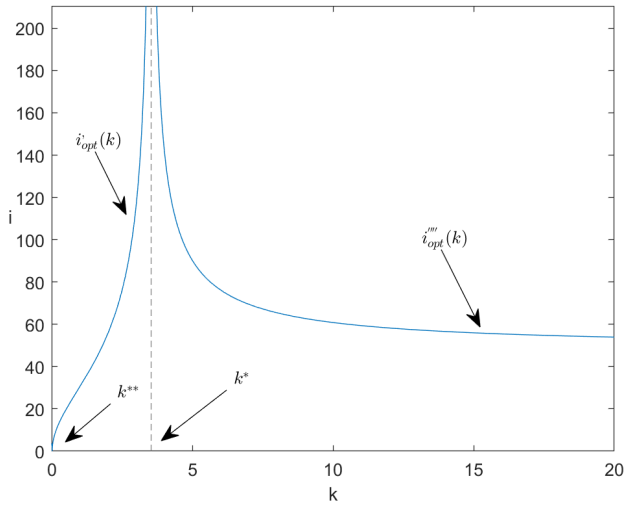

Figure 3.2: *Problem 1a*: optimum locus in the i-k plane, as expressed by Equation 3.35

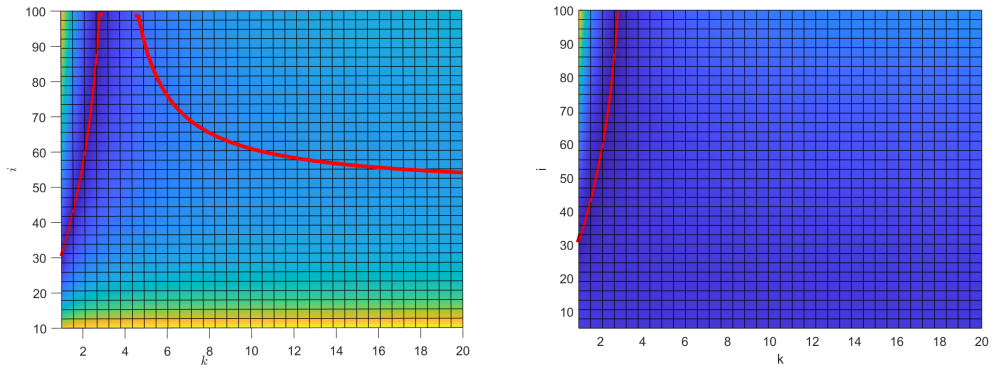

(a) (b)

Figure 3.3: *Problem 1a*: (a) $C_{m,RMS}$ in i-k plane. In red, the optimum locus of Equation 3.35. (b) $P_{m,RMS}$ in i-k plane. In red, the optimum locus of Equation 3.30.

Usually, the most commonly used p-norms are the Root Mean Square (RMS), obtained with $p = 2$, and the Maxmimum (MAX), obtained with $p = \infty$.

The definition of the function F heavily depends on the application. One can decide to optimize energy consumption, motor range of motion, motor speed, or even take into consideration the actuator control loop and optimize with respect to, for example, closed-loop bandwidth, phase margin, settling time overshoot and so on. However, the most common choices for F are the motor torque $C_m(t)$ or motor power $P_m(t)$ defined as:

$$P_m(t) = C_m(t)\dot{\theta}_m(t) \tag{3.11}$$

Due to the more complicated equations arising from having multiple degrees of freedom and more design parameters, the solution of the optimization problem will be heavily dependent on the output imposed motion trajectory $\theta_l(t)$.

The problem can be solved numerically for any given $\theta_l(t)$ and $C_{ext}(t)$. However, here we present the analytic solution of the problem employing two commonly used trajectories for point-to-point motion, the cycloidal trajectory:

$$\theta_{l,cycloidal}(t) = A\left[\frac{t}{t_a} - \frac{\sin\left(\frac{2\pi t}{t_a}\right)}{2\pi}\right] \tag{3.12}$$

and the Freudenstein 1-3 trajectory:

$$\theta_{l,Freudenstein\ 1-3}(t) = A\left[\frac{t}{t_a} - 27\frac{\sin\left(\frac{2\pi t}{t_a}\right)}{56\pi} - \frac{\sin\left(\frac{6\pi t}{t_a}\right)}{168\pi}\right] \tag{3.13}$$

where A is the amplitude of the point-to-point motion and t_a is the motion duration. Figure 3.1 shows a comparison of cycloidal (blue) and Freudenstein 1-3 (red) trajectories up to the jerk (4th derivative).

For simplicity in the following we will neglect external torques ($C_{ext}(t) = 0$), friction and inertial effects of the compliant elements, but of course these phenomena can be taken into consideration when solving the problem numerically. The analytical solution will be derived for both SEA and DEA.

Hence, we define the following problems:

1. *Problem 1a*: Given SEA model developed in Section 2.7 find optimal i, k given zero external torque and Cycloidal trajectory output motion:

$$C_{ext}(t) = 0 \qquad \theta_l(t) = \theta_{l,cycloidal}(t) \tag{3.14}$$

with respect to $C_{m,RMS}$ and $P_{m,RMS}$.

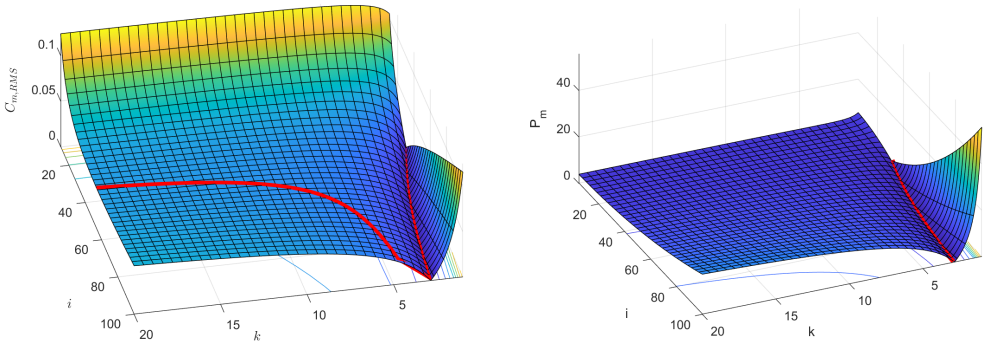

(a) (b)

Figure 3.4: *Problem 1a*: (a) 3D surface representation of $C_{m,RMS}$. In red, the optimum locus of Equation 3.35. (b) 3D surface representation of $P_{m,RMS}$. In red, the optimum locus of Equation 3.30.

2. *Problem 1b*: Given SEA model developed in Section 2.7 find optimal i, k given zero external torque and Freudenstein 1-3 trajectory output motion:
$$C_{ext}(t) = 0 \qquad \theta_l(t) = \theta_{l,Freudenstein\ 1-3}(t) \tag{3.15}$$
with respect to $C_{m,RMS}$ and $P_{m,RMS}$.

3. *Problem 2a*: Given DEA model developed in Section 2.8 find optimal i, k given zero external torque and Cycloidal trajectory output motion:
$$C_{ext}(t) = 0 \qquad \theta_l(t) = \theta_{l,cycloidal}(t) \tag{3.16}$$
with respect to $C_{m,RMS}$ and $P_{m,RMS}$.

4. *Problem 2b*: Given DEA model developed in Section 2.8 find optimal i, k given zero external torque and Freudenstein 1-3 trajectory output motion:
$$C_{ext}(t) = 0 \qquad \theta_l(t) = \theta_{l,Freudenstein\ 1-3}(t) \tag{3.17}$$
with respect to $C_{m,RMS}$ and $P_{m,RMS}$.

3.3.1 SEA optimization

Referring to the SEA model developed in Section 2.7 and schematized in Figure 2.5, we have already obtained the expression for motor position $\theta_m(t)$ in Equation 2.86 and for motor torque $C_m(t)$ in Equation 2.87.

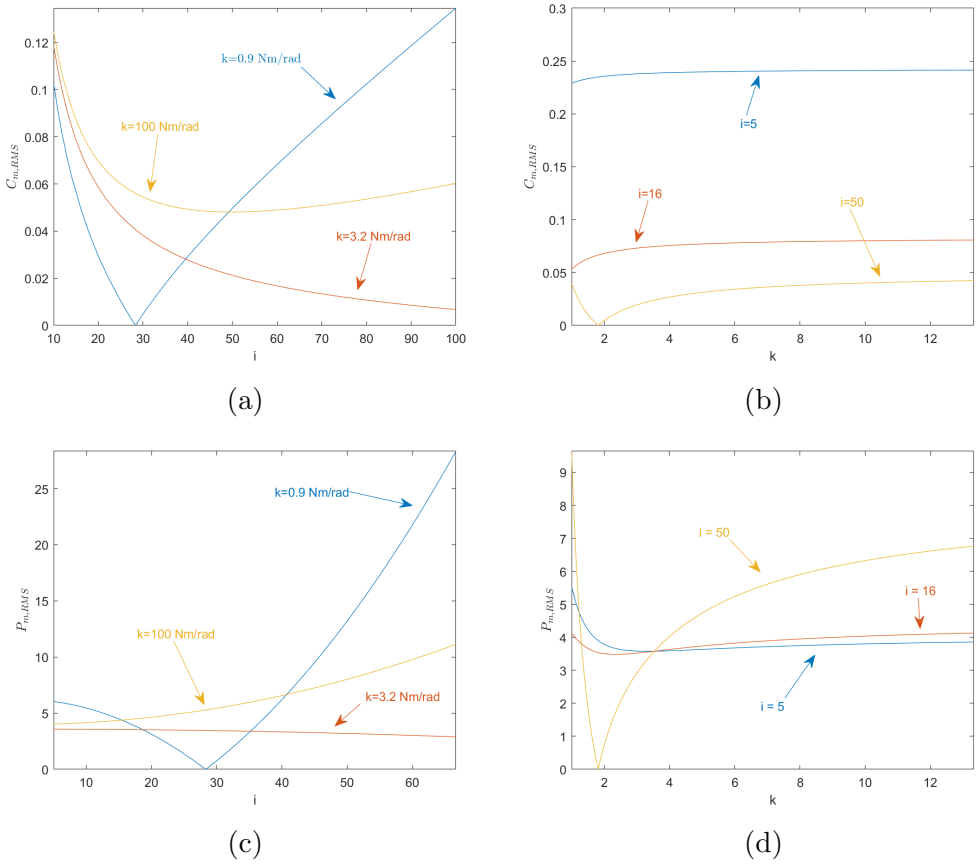

Figure 3.5: *Problem 1a*: (a): $C_{m,RMS}$ plotted for different values of k. Both $k = 0.9$ Nm/rad and $k = 3.2$ Nm/rad belong to the $[k^{**},\ k^{*}]$ interval, whereas $k = 100$ doesn't, despite being closer to compliances found in practical SEA designs. (b) $C_{m,RMS}$ plotted for different values of i. For $i = 50$ the common implementation is with Harmonic Drives (HD). For $i = 16$ and $i = 5$ the commonly adopted solution is planetary gearboxes. (c) $P_{m,RMS}$ plotted for the same values of k as in (a). (d) $P_{m,RMS}$ plotted for the same values of i as in (b).

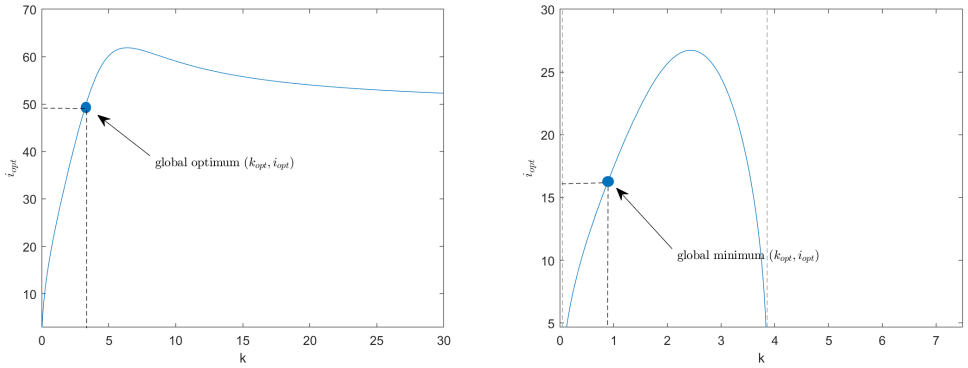

(a) (b)

Figure 3.6: *Problem 1b*: optimum locus in the i-k plane with Freudenstein 1-3 output motion trajectory with respect to (a) $C_{m,RMS}$, solution of Equation 3.46 (b) $P_{m,RMS}$, solution of Equation 3.47. The global minima are also shown.

Cycloidal Trajectory

If we substitute in Equations 2.86 and 2.87 the conditions enforced by the definition of *Problem 1a* we obtain:

$$\dot{\theta}_m(t) = \frac{Ai}{kt_a^3}\left[\cos\left(\frac{2\pi t}{t_a}\right)\left(kt_a^2 - 4J_l\pi^2\right) - kt_a^2\right] \tag{3.18}$$

And

$$C_m(t) = -\frac{2A\ \pi \sin\left(\frac{2\pi t}{t_a}\right)\sigma}{ikt_a^4} \tag{3.19}$$

With

$$\sigma = J_g\, k\, {t_a}^2 - 4\, J_g\, J_l\, \pi^2 + J_l\, k\, {t_a}^2 - 4\, J_l\, J_m\, i^2\, \pi^2 + J_m\, i^2\, k\, {t_a}^2 \tag{3.20}$$

The expression for $P_m(t)$ follows directly from Equation 3.11 and is not reported for brevity.

We proceed by computing the two objective functions

$$C_{m,RMS}\,(i,k) = \sqrt{\frac{1}{t_a}\int_0^{t_a} C_m^2(t)dt} \tag{3.21}$$

$$= \dots$$

$$= \frac{\sqrt{2}A\pi\,|\sigma|}{ikt_a^4} \tag{3.22}$$

And

$$P_{m,RMS}(i,k) = \sqrt{\frac{1}{t_a}\int_0^{t_a} P_m^2(t)dt} \tag{3.23}$$

$$= \dots$$

$$= \frac{\sqrt{2}A^2\pi\left|\sigma\right|\sqrt{16\pi^4 J_l^2 - 8\pi^2 J_l k t_a^2 + 5k^2 t_a^4}}{2k^2 t_a^7} \tag{3.24}$$

Let's first analyze Equation 3.22 trying to find its, possibly multiple, minima.

We can always write

$$C_{m,RMS}(i,k) = \begin{cases} 0 & \sigma = 0 \\ \dfrac{\sqrt{2}A\pi\sigma}{t_a^4 ki} \triangleq F_1^{'} > 0 & \sigma > 0 \\ -\dfrac{\sqrt{2}A\pi\sigma}{t_a^4 ki} \triangleq F_1^{''} > 0 & \sigma < 0 \end{cases} \tag{3.25}$$

Looking at Equation 3.22, since $C_{m,RMS} \geq 0$ then it's obvious that if σ is zero for some i, k, we found a local minima for which the objective function is optimized.

We then rewrite Equation 3.20 imposing $\sigma = 0$:

$$i^2\left(J_m k t_a^2 - 4J_m J_l \pi^2\right) + k\left(J_g t_a^2 + J_l t_a^2\right) - 4J_g J_l \pi^2 = 0 \tag{3.26}$$

From which:

$$k^{'}(i) = \frac{4J_l\pi^2\left(J_g + J_m i^2\right)}{t_a^2\left(J_m i^2 + J_g + J_l\right)} \tag{3.27}$$

Equation 3.27 exists $\forall i \in \mathbb{R}$, is even, and therefore symmetric with respect to the k axis, and is always greater than zero. Moreover:

$$\lim_{i\to\infty} k^{'}(i) = \lim_{i\to-\infty} k^{'}(i) = \frac{4J_l\pi^2}{ta^2} \triangleq k^* \tag{3.28}$$

And:

$$k^{'}(0) = \frac{4J_l\pi^2 J_g}{t_a^2\left(J_g + J_l\right)} \triangleq k^{**} < k^* \tag{3.29}$$

We can conclude that the codomain of $k^{'}$ is the interval $[k^{**}, k^*]$. Looking at this result from another perspective, we can conclude that if k belongs to

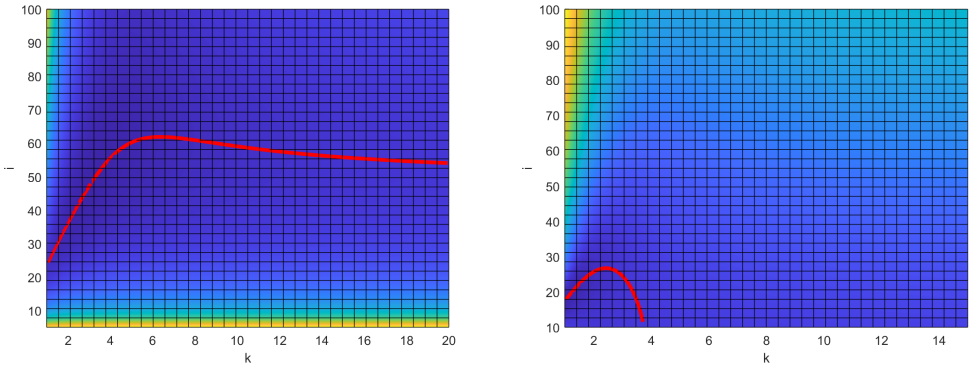

(a) (b)

Figure 3.7: *Problem 1b*: (a) $C_{m,RMS}$ in i-k plane. In red, the optimum locus of Equation 3.46. (b) $P_{m,RMS}$ in i-k plane. In red, the optimum locus of Equation 3.47.

the set $[k^{**}, k^{*}]$ it's always possible to find an optimal i, given by the solution of $\sigma = 0$ with respect to i:

$$i'_{opt}(k) = \sqrt{\frac{4J_g J_l \pi^2 - k t_a^2 \left(J_g + J_l\right)}{J_m \left(k t_a^2 - 4 J_l \pi^2\right)}} \tag{3.30}$$

such that $\sigma = 0$, and as a consequence also $C_{m,RMS}\left(i,k\right) = 0$, which is an obvious minimum since $C_{m,RMS}\left(i,k\right) \geq 0$ by definition. If, on the contrary, k is selected outside the interval $[k^{**}, k^{*}]$, no i exists that makes σ, and therefore $C_{m,RMS}\left(i,k\right)$, being equal to zero.

Outside the particular case $\sigma = 0$, we need to solve the systems of equations

$$\begin{cases} \dfrac{\partial F_1'\left(i,k,\right)}{\partial i} = 0 \\ \dfrac{\partial F_1'\left(i,k,\right)}{\partial k} = 0 \end{cases} \quad and \quad \begin{cases} \dfrac{\partial F_1''\left(i,k,\right)}{\partial i} = 0 \\ \dfrac{\partial F_1''\left(i,k,\right)}{\partial k} = 0 \end{cases} \tag{3.31}$$

restricted to their particular domain. However, no solution is found for either of the two systems of Equation 3.31, hence we can conclude that function $C_{m,RMS}$ has no critical points and therefore no isolated minima. Since no critical points exist, we drop one of the dependency from both variables i and k and search for optima loci parametrized by one of the two. We choose to drop the dependency on k, and therefore solve:

$$\frac{dF_1'\left(i\right)}{di} = 0 \tag{3.32}$$

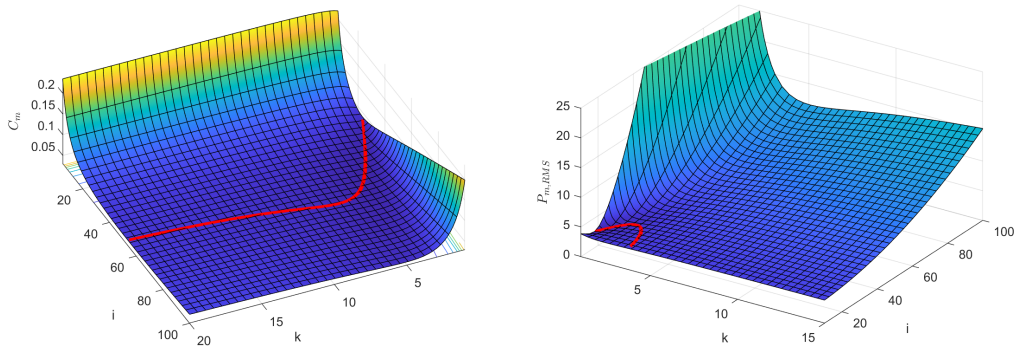

(a) (b)

Figure 3.8: *Problem 1b*: (a) 3D surface representation of $C_{m,RMS}$. In red, the optimum locus of Equation 3.46. (b) 3D surface representation of $P_{m,RMS}$. In red, the optimum locus of Equation 3.47.

and:

$$\frac{dF_1''(i)}{di} = 0 \tag{3.33}$$

The solution for both Equation 3.32 and Equation 3.33 in their respective domains is given by:

$$i''_{opt}(k) = \sqrt{-\frac{4J_gJ_l\pi^2 - kt_a^2(J_g + J_l)}{J_m(kt_a^2 - 4J_l\pi^2)}} \tag{3.34}$$

The expression for $C_{m,RMS}$ at $(i_{opt}(k), k)$ can be computed via simple substitution. Putting together the results obtained so far, in particular Equations 3.30 and 3.34, the complete optimum locus with respect to $C_{m,RMS}$, is given by:

$$i_{opt}(k) = \sqrt{\left|\frac{4J_gJ_l\pi^2 - kt_a^2(J_g + J_l)}{J_m(kt_a^2 - 4J_l\pi^2)}\right|} \tag{3.35}$$

For which:

$$C_{m,RMS}(i_{opt}, k) = \begin{cases} 0 & \text{if } k^{**} < k < k^* \\ C_{m,RMS,opt} & \text{otherwise} \end{cases} \tag{3.36}$$

with:

$$C_{m,RMS,opt} = \frac{4\pi A\sqrt{J_m(kt_a^2 - 4J_l\pi^2)\left[(J_g + J_l)kt_a^2 - 4J_gJ_l\pi^2\right]}}{\sqrt{2}kt_a^2} \tag{3.37}$$

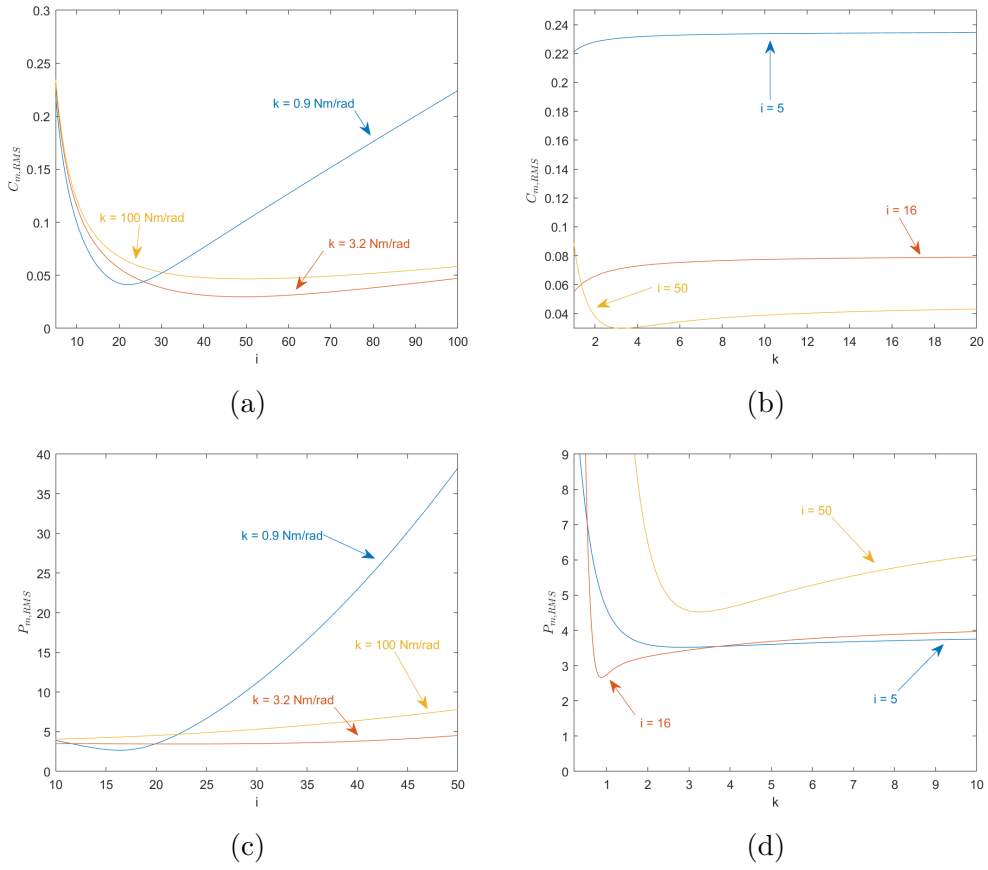

Figure 3.9: *Problem 1b*: (a): $C_{m,RMS}$ plotted for different values of k. For all three values of k it is possible to obtain a minimum. No i, k values produce a zero $C_{m,RMS}$. (b) $C_{m,RMS}$ plotted for different values of i. (c) $P_{m,RMS}$ plotted for the same values of k as in (a). Only for $k = 0.9$ Nm/rad it is possible to determine a minium for $P_{m,RMS}$. (d) $P_{m,RMS}$ plotted for the same values of i as in (b). All minima exist for small values of k.

We now switch our attention to Equation 3.24. We recognize a structure similar to Equation 3.22. First of all, we notice that the numerator can only be zero if and only if $\sigma = 0$, since the equation:

$$16\pi^4 J_l^2 - 8\pi^2 J_l k t_a^2 + 5k^2 t_a^4 = 0 \tag{3.38}$$

has no solution for $k \in \mathbb{R}$. Hence we can write, as before:

$$P_{m,RMS}(i,k) = \begin{cases} 0 & \sigma = 0 \\ \dfrac{\sqrt{2}A^2\pi\,|\sigma|\,\sqrt{16\pi^4 J_l^2 - 8\pi^2 J_l k t_a^2 + 5k^2 t_a^4}}{2k^2 t_a^7} \triangleq F_2^{'} > 0 & \sigma > 0 \\ -\dfrac{\sqrt{2}A^2\pi\,|\sigma|\,\sqrt{16\pi^4 J_l^2 - 8\pi^2 J_l k t_a^2 + 5k^2 t_a^4}}{2k^2 t_a^7} \triangleq F_2^{''} > 0 & \sigma < 0 \end{cases} \tag{3.39}$$

Since σ is always defined by Equation 3.20, the same results obtained before apply: if k belongs to the set $[k^{**}, k^*]$ it's always possible to find an optimal i given by 3.30 such that $\sigma = 0$, and as a consequence also $P_{m,RMS}(i,k) = 0$, whereas if k is selected outside the interval $[k^{**}, k^*]$, no i exists that makes σ, and $P_{m,RMS}(i,k)$, being equal to zero. Again, the system

$$\begin{cases} \dfrac{\partial F_2^{'}(i,k,)}{\partial i} = 0 \\ \dfrac{\partial F_2^{'}(i,k,)}{\partial k} = 0 \end{cases} \quad and \quad \begin{cases} \dfrac{\partial F_2^{''}(i,k,)}{\partial i} = 0 \\ \dfrac{\partial F_2^{''}(i,k,)}{\partial k} = 0 \end{cases} \tag{3.40}$$

gives no solution.

However, in this case, also:

$$\frac{dF_2^{'}(i)}{di} = 0 \tag{3.41}$$

and:

$$\frac{dF_2^{''}(i)}{di} = 0 \tag{3.42}$$

have no solution.

We can finally conclude that, if $k^{**} < k < k^*$, the optimum locus with respect to $P_{m,RMS}$ is given by Equation 3.30 and in this domain $P_{m,RMS} = 0$. On the other hand, no minimum exists for $P_{m,RMS}$ in the ranges $k \leq k^{**}$ and $k \geq k*^*$.

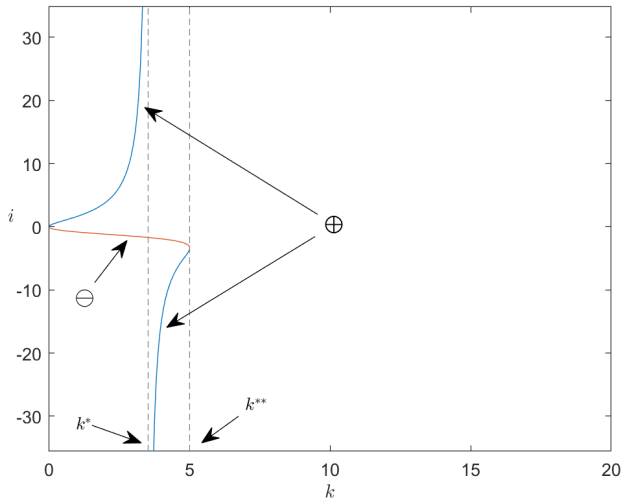

Figure 3.10: *Problem 2a*: loci in the i-k plane where $\eta = 0$ given by Equation 3.54. The " $-$ " is always negative whereas the " $+$ " locus is positive only for $0 < k < k^*$. *Remark:* In this figure the value of J_m is modified to empathize the difference between k^* and k^{**}, that in practical cases are normally very similar.

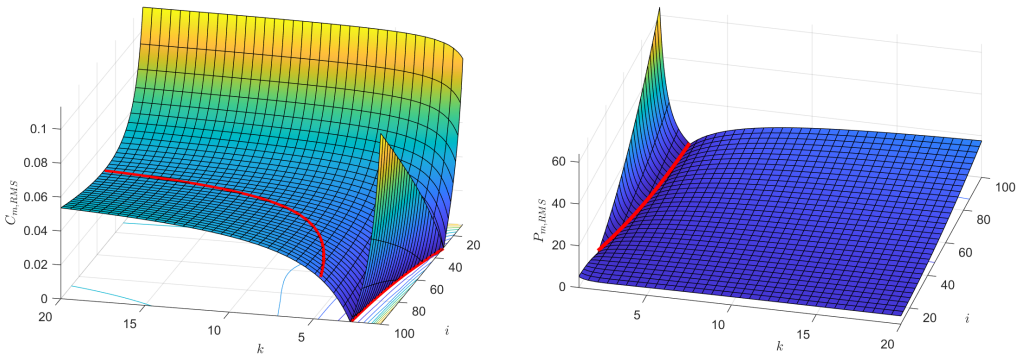

(a) (b)

Figure 3.11: *Problem 2a*: (a) 3D surface representation of $C_{m,RMS}$. (b) 3D surface representation of $P_{m,RMS}$. In red, the optimum loci.

Freudenstein 1-3 Trajectory

We give now another example of optimization applied to SEA. In particular, we focus our attention on the conditions enforced by *Problem 1b*. The solution of *Problem 1b* follows the same procedure previously outlined, but most of the obtained expressions are extremely complex and are not reported here for brevity.

We begin again by enforcing the conditions imposed by the problem into 2.86 and 2.87, and then compute the RMS functions $C_{m,RMS}(i,k)$ and $P_{m,RMS}(i,k)$ as in, respectively, 3.21 and 3.23.

We then try to find critical points by solving

$$\begin{cases} \dfrac{\partial C_{m,RMS}\,(i,k,)}{\partial i} = 0 \\ \dfrac{\partial C_{m,RMS}\,(i,k,)}{\partial k} = 0 \end{cases} \tag{3.43}$$

and, in this case, we indeed find a solution:

$$\begin{cases} i_{opt} = \sqrt{\dfrac{J_g + J_l}{J_m}} \\ k_{opt} = \dfrac{18 J_l \pi^2 \,(2J_g + J_l)}{5 t_a^2 \,(J_g + J_l)} \end{cases} \tag{3.44}$$

which represents a global interior minimum of $C_{m,RMS}$.

The same happens if we try to solve

$$\begin{cases} \dfrac{\partial P_{m,RMS}\,(i,k,)}{\partial i} = 0 \\ \dfrac{\partial P_{m,RMS}\,(i,k,)}{\partial k} = 0 \end{cases} \tag{3.45}$$

we find a global interior minimum (i_{opt}, k_{opt}) for $P_{m,RMS}$, whose expression is not reported here.

A minimum locus $i_{opt}(k)$ exists for both $C_{m,RMS}$ and $C_{m,RMS}$, and can be obtained by solving:

$$\frac{d}{di} C_{m,RMS}\,(i) = 0 \tag{3.46}$$

and:

$$\frac{d}{di} P_{m,RMS}\,(i) = 0 \tag{3.47}$$

even though the second exists only for very small values of k.

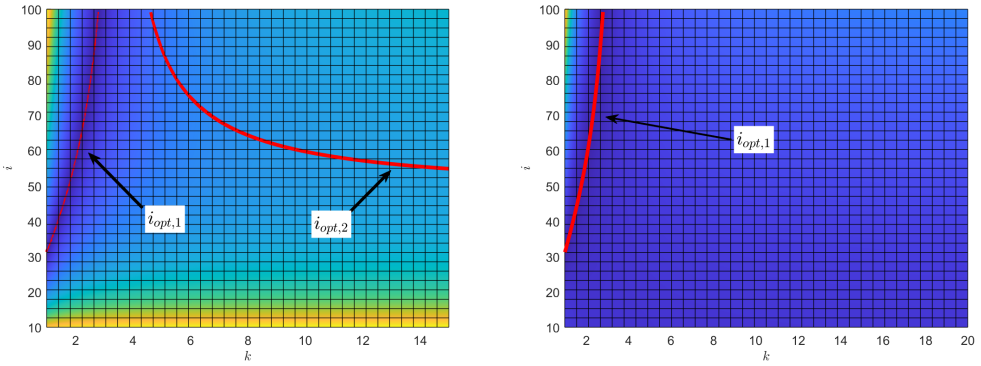

(a) (b)

Figure 3.12: *Problem 2a*: (a) $C_{m,RMS}$ in i-k plane. In red, the optimum locus of Equation 3.58. Along $i_{opt,1}$ $C_{m,RMS}$ is zero whereas along $i_{opt,2}$ $C_{m,RMS} > 0$ with optimal i,k values. (b) $P_{m,RMS}$ in i-k plane. In red, the optimum locus $i_{opt,1}$ along which $C_{m,RMS}$, and consequently $P_{m,RMS}$, is zero.

3.3.2 SEA Numerical example

To have better insights of what was developed in the last analytic examples, and to better investigate the sensitivity of motor requirements on SEA transmission ratio and spring stiffness, a numerical case study is presented. Parameters are taken from Table 3.1. Results from numerical analysis of both *Problem 1a* and *Problem 1b* are presented in the following.

Concerning *Problem 1a*, Figure 3.2 shows the optimum locus of the reduction ratio i with respect to compliance k expressed in Equation 3.35.

The first branch $i'_{opt}(k)$ is delimited by k^{**} and k^{*}, that in this example are equal to:

$$k^{**} = 0.02 \text{ Nm/rad} \qquad k^{*} = 3.53 \text{ Nm/rad}$$

Along $i'_{opt}(k)$ both $C_{m,RMS}$ and $P_{m,RMS}$ are zero.

The second branch $i''_{opt}(k)$ exists for $k > k^{*}$ and $k < k^{**}$. Curve $i''_{opt}(k)$ represents the locus of the optimal i for a given k with respect to $C_{m,RMS}$, but with $C_{m,RMS} > 0$. This locus does not exist for $P_{m,RMS}$.

These conclusions can be drawn from Figure 3.3, that shows the same locus presented in Figure 3.2 with superimposed the values of $C_{m,RMS}(i,k)$ and $P_{m,RMS}(i,k)$, in Figure 3.3a and Figure 3.3b respectively.

Figure 3.4 shows the same information, but plotted as a 3D surface for better visualization.

As predicted by the equations previously derived, the required RMS motor torque and power can be zero for $k^{**} < k < k^{*}$. For any fixed value of

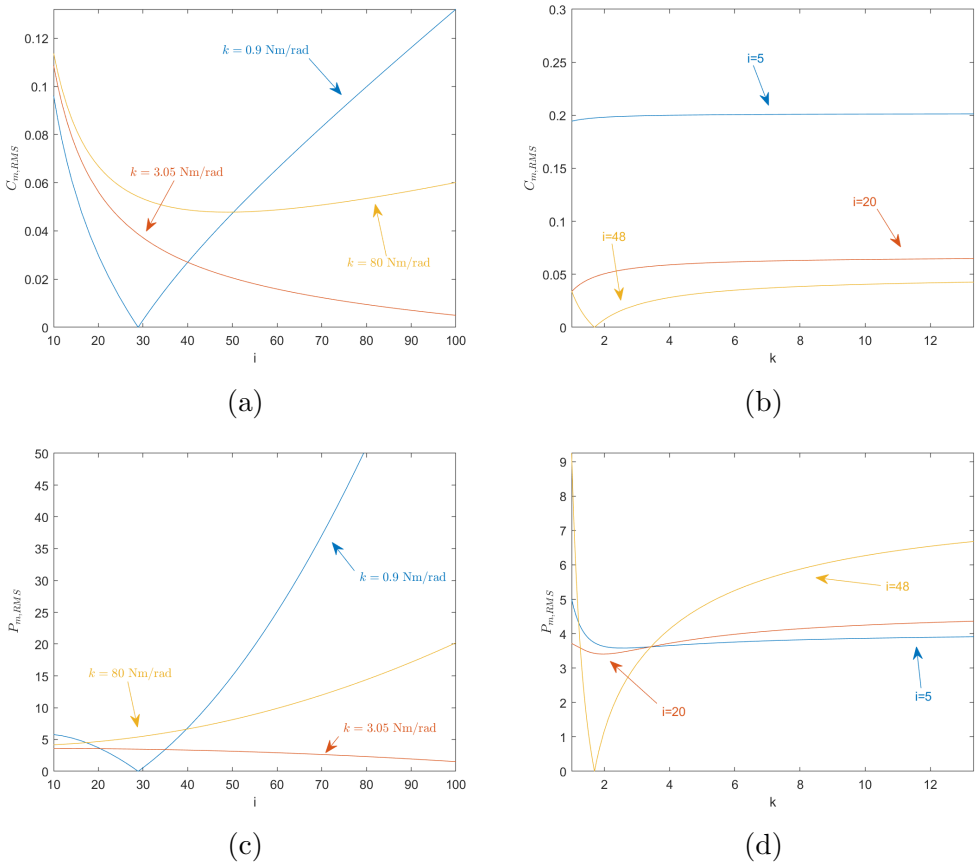

Figure 3.13: *Problem 2a*: (a): $C_{m,RMS}$ plotted for different values of k. Both $k = 0.9$ Nm/rad and $k = 3.05$ Nm/rad belong to the $[0,\ k^*]$ interval, whereas $k = 100$ doesn't. (b) $C_{m,RMS}$ plotted for different values of i. (c) $P_{m,RMS}$ plotted for the same values of k as in (a). (d) $P_{m,RMS}$ plotted for the same values of i as in (b).

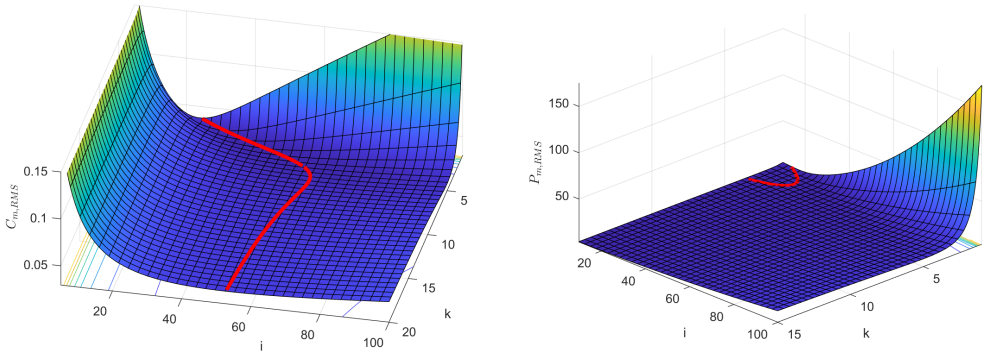

(a) (b)

Figure 3.14: *Problem 2b*: (a) 3D surface representation of $C_{m,RMS}$. (b) 3D surface representation of $P_{m,RMS}$. In red, the optimum loci.

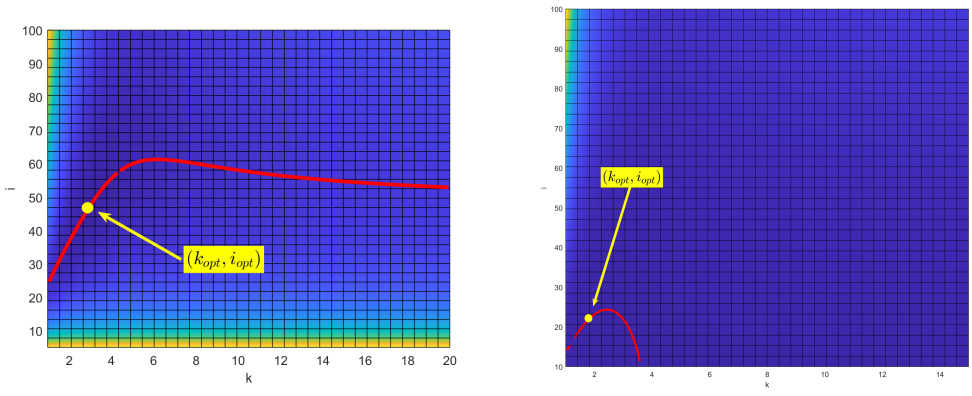

(a) (b)

Figure 3.15: *Problem 2b*: (a) $C_{m,RMS}$ in i-k plane. (b) $P_{m,RMS}$ in i-k plane. In red, the optimum loci

k in one of the ranges $k \leq k^{**}$ and $k \geq k^{*}$ there always exists an optimum value for the transmission ratio, $i_{opt}(k)$, that minimizes $C_{m,RMS}$, while no such optima exist for $P_{m,RMS}$.

To better highlight the dependencies of motor requirements on transmission parameters, Figures 3.5a and 3.5c report, respectively, $C_{m,RMS}$ and $P_{m,RMS}$ as functions of i for three values of k. For $k = 0.9$ Nm/rad and $k = 3.2$ Nm/rad both $C_{m,RMS}$ and $P_{m,RMS}$ admit a zero, even though since $k = 3.2$ Nm/rad is close to k^{*} the zero occurs for very high values of i. For $k = 100$ Nm/rad, no zero can be obtained for either $C_{m,RMS}$ or $P_{m,RMS}$, but $C_{m,RMS}$ admits an interior minimum, whereas $P_{m,RMS}$ doesn't.

Similarly, Figures 3.5b and 3.5d show, respectively, $C_{m,RMS}$ and $P_{m,RMS}$ as functions of k for three selected values of i, where $i = 50$ can be found in practical SEA implementations employing HD (Harmonic Drive) transmission, whereas $i = 16$ and $i = 5$ can be easily realized with one/two-stage planetary gearboxes. The case $i = 5$ is also close to the direct-drive condition.

Concerning *Problem 1b*, a global minimum exists for $C_{m,RMS}$, as given by Equation 3.44:

$$i_{opt} \approx 50 \qquad k_{opt} \approx 3.4 \text{ Nm/rad} \qquad C_{m,RMS} \approx 0.03 \text{ Nm}$$

and a different global minimum exists for $P_{m,RMS}$, obtained from the solution of 3.45:

$$i_{opt} \approx 16 \qquad k_{opt} \approx 0.9 \text{ Nm/rad} \qquad P_{m,RMS} \approx 2.6 \text{ W}$$

The locus of optimum i as function of k, $i_{opt}(k)$ for $C_{m,RMS}$ and $P_{m,RMS}$, derived form Equation 3.46 and Equation 3.47, respectively, are shown in Figure 3.6, together with the global minima.

Figure 3.7 shows the same loci presented in Figure 3.6, with superimposed the values of $C_{m,RMS}(i,k)$ and $P_{m,RMS}(i,k)$, whereas Figure 3.8 show the same results as 3D surfaces. As shown, no zero exists for RMS motor torque and power. For any fixed value of k there always exist an optimum value of the transmission ratio $i_{opt}(k)$ minimizing $C_{m,RMS}$, whereas interior optima exist for $P_{m,RMS}$ only for small values of k.

A comparison analogous of that of Figure 3.5 can be found in Figure 3.9.

The different shapes of $C_{m,RMS}$ and $P_{m,RMS}$ reported in Figure 3.4a versus Figure 3.8a and in Figure 3.4b versus Figure 3.8b underline the influence of the load trajectory profile on both motor requirements and optimal transmission parameters. In particular, comparison of Figures 3.5 with Figures 3.9 highlights that motor torque and power are significantly affected by the chosen load trajectory whenever the transmission is required to be compliant (namely, for low-to-medium values of k).

3.3.3 DEA optimization

Referring to the DEA model developed in Section 2.8 and schematized in Figure 2.6, we have already obtained the approximated expressions for motor position $\theta_m(t)$ in Equation 2.122 and for motor torque $C_m(t)$ in Equation 2.123.

Cycloidal Trajectory

If we substitute in Equations 2.122 and 2.123 the conditions enforced by the definition of *Problem 2a* we obtain:

$$\dot{\theta}_m(t) = A + A\frac{4kt_a^2 J_l i^2 \pi^2 - k^2 (i+1)^2 t_a^4 + 16 J_l J_s i \pi^4 (i+1)}{k^2 (i+1) t_a^5} \cos\left(\frac{2\pi t}{t_a}\right) \tag{3.48}$$

And

$$C_m(t) = \frac{2\pi A \eta}{k t_a^4 (i+1)} \sin\left(\frac{2\pi t}{t_a}\right) \tag{3.49}$$

With

$$\eta = J_l k t_a^2 + J_m k t_a^2 (i+1)^2 - 4\pi^2 J_m J_l i^2 \tag{3.50}$$

The expression for $P_m(t)$ follows again from Equation 3.11 and is not reported for brevity.

We proceed by computing the two objective functions

$$C_{m,RMS}(i,k) = \frac{\sqrt{2}\pi A |\eta|}{k (i+1) t_a^4} \tag{3.51}$$

And

$$P_{m,RMS}(i,k) = \sqrt{\frac{1}{t_a}\int_0^{t_a} P_m^2(t) dt} \tag{3.52}$$

The analysis of Equation 3.51 follows the same procedure outlined for SEAs. Of course for Equation 3.51 $C_{m,RMS} \geq 0$ and $C_{m,RMS} = 0$ only if $\eta = 0$. Solving:

$$\eta = J_l k t_a^2 + J_m k t_a^2 (i+1)^2 - 4\pi^2 J_m J_l i^2 = 0 \tag{3.53}$$

with respect to i allows us to find the locus of (i,k) points that allow zeroing of motor RMS power. From Equation 3.50 it follows that

$$i_{opt}(k) = \frac{J_m k t_a^2 \pm t_a \sqrt{k J_m J_l \left[4\pi^2 (J_m + J_l) - k t_a^2\right]}}{J_m (4 J_l \pi^2 - k t_a^2)} \tag{3.54}$$

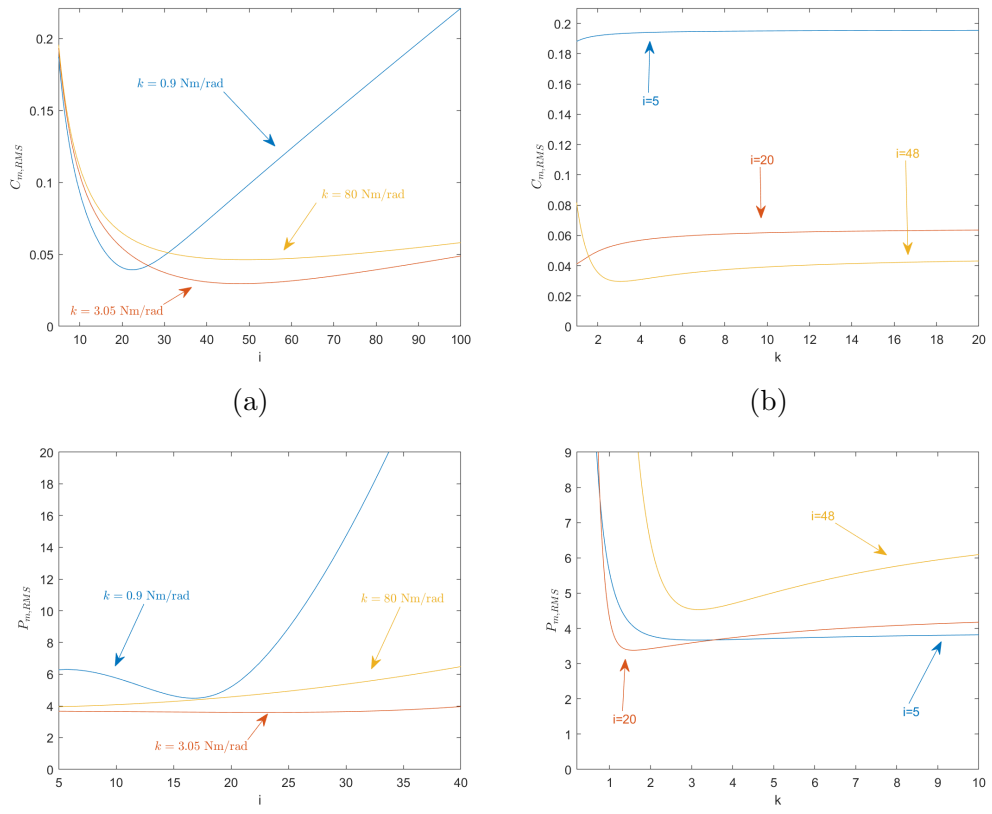

Figure 3.16: *Problem 2b*: (a): $C_{m,RMS}$ plotted for different values of k. For all three values of k it is possible to obtain a minimum. No i, k values produce a zero $C_{m,RMS}$. (b) $C_{m,RMS}$ plotted for different values of i. (c) $P_{m,RMS}$ plotted for the same values of k as in (a). Only for $k = 0.9$ Nm/rad it is possible to determine a minium for $P_{m,RMS}$. (d) $P_{m,RMS}$ plotted for the same values of i as in (b). All minima exist for small values of k.

which exists for $[0 < k < k^*] \bigcup [k^* < k < k^{**}]$ with

$$k^* = \frac{4J_l\pi^2}{t_a^2} \qquad k^{**} = \frac{4\pi^2\left(J_m + J_l\right)}{t_a^2} \tag{3.55}$$

However, if we analyze Equation 3.54 we find that the "$-$" solution is always negative in its domain, while the "$+$" solution is positive only in the interval $[0 < k < k^*]$. Threfore we can conclude that if $0 < k < k^*$ it's always possible to find an optimal i give by:

$$i_{opt}(k) = \frac{J_m k t_a^2 + t_a\sqrt{kJ_mJ_l\left[4\pi^2\left(J_m + J_l\right) - kt_a^2\right]}}{J_m\left(4J_l\pi^2 - kt_a^2\right)} \tag{3.56}$$

such that η, and consequently also $C_{m,RMS}$ and $P_{m,RMS}$ are zero. Outside this interval, no zeroing of these functions is possible.

Following the same approach used for SEAs we search for the locus of minima of i as function of k by solving:

$$\frac{dC_{m,RMS}(i)}{di} = 0 \tag{3.57}$$

The solution of Equation 3.57, whose steps are not reported for brevity, brings the following set of results:

$$i_{opt}(k) = \begin{pmatrix} \dfrac{J_m k t_a^2 + t_a\sqrt{kJ_mJ_l\left[4\pi^2\left(J_m + J_l\right) - kt_a^2\right]}}{J_m\left(4J_l\pi^2 - kt_a^2\right)} \\ \dfrac{J_m k t_a^2 - t_a\sqrt{kJ_mJ_l\left[4\pi^2\left(J_m + J_l\right) - kt_a^2\right]}}{J_m\left(4J_l\pi^2 - kt_a^2\right)} \\ \dfrac{J_m\left(kt_a^2 - 4J_l\pi^2\right) + \sqrt{J_mJ_l\left(4J_l\pi^2 - kt_a^2\right)\left(4J_m\pi^2 - kt_a^2\right)}}{J_m\left(4J_l\pi^2 - kt_a^2\right)} \\ \dfrac{J_m\left(kt_a^2 - 4J_l\pi^2\right) - \sqrt{J_mJ_l\left(4J_l\pi^2 - kt_a^2\right)\left(4J_m\pi^2 - kt_a^2\right)}}{J_m\left(4J_l\pi^2 - kt_a^2\right)} \end{pmatrix} \tag{3.58}$$

However, solution (2) and (3) in 3.58 are always negative $\forall k \in \mathbb{R}$, whereas solution (1) is the same of Equation 3.56 (which is positive for $0 < k < k^*$) while solution (4) is positive for $k > k^*$.

So overall, the optimum locus $i_{opt}(k)$ is given by:

$$i_{opt}(k) = \begin{cases} \dfrac{J_m k t_a^2 + t_a\sqrt{kJ_mJ_l\left[4\pi^2\left(J_m + J_l\right) - kt_a^2\right]}}{J_m\left(4J_l\pi^2 - kt_a^2\right)} & \text{if } 0 < k < k^* \\ \dfrac{J_m\left(kt_a^2 - 4J_l\pi^2\right) - \sqrt{J_mJ_l\left(4J_l\pi^2 - kt_a^2\right)\left(4J_m\pi^2 - kt_a^2\right)}}{J_m\left(4J_l\pi^2 - kt_a^2\right)} & \text{if } k > k^* \end{cases} \tag{3.59}$$

Concerning the minimization problem of Equation 3.52, we already know that along the locus described by Equation 3.54 $C_{m,RMS}$ is zero and therefore also $P_{m,RMS}$ is zero. We can conclude that Equation 3.54 represents a minimum locus also for $P_{m,RMS}$ since $P_{m,RMS} \geq 0$. Analyzing 3.52 with the same tools employed before, we would find that Equation 3.54 is the only optimum locus in the $k - i$ plane.

Freudenstein 1-3 Trajectory

Focusing our attention on *Problem 2b*, the solution starts again by enforcing the conditions imposed by the problem into 2.122 and 2.123, and then compute the RMS functions $C_{m,RMS}(i,k)$ and $P_{m,RMS}(i,k)$. For reference, here we report the expression only of $C_m(t)$ after the substitution:

$$C_m(t) = \frac{6A\pi\gamma\left[36J_lJ_mi^2\pi^2\left(\gamma^2-1\right) - kt_a^2\left(\gamma^2-3\right)\left(J_mi^2+2J_mi+J_m+J_l\right)\right]}{7kt_a^4\left(i+1\right)} \tag{3.60}$$

with

$$\gamma = \sin\left(\frac{2\pi t}{t_a}\right)$$

The expression of $\dot{\theta}_m(t)$, $C_{m,RMS}$ and $P_{m,RMS}$ are omitted for brevity. The results of the analysis are similar to the SEA case. No zeroing of torque and/or power is possible, a global minimum for $C_{m,RMS}$ exists and is given by:

$$\begin{cases} i_{opt} = \dfrac{\sqrt{J_l} - \sqrt{J_m}}{\sqrt{J_m}} \\ k_{opt} = \dfrac{18\pi^2\left(J_m + J_l - 2\sqrt{J_mJ_l}\right)}{5t_a^2} \end{cases} \tag{3.61}$$

and a global minimum exists also for $P_{m,RMS}$ exists but the expression is not reported. Minima loci $i_{opt}(k)$ can be obtained, but are not reported here for brevity.

3.3.4 DEA Numerical example

A numerical analysis was conducted on the results obtained for DEAs as has been previously done for SEAs. Numerical parameters are summarized in Table 3.1. Results from numerical analysis of both *Problem 2a* and *Problem 2b* are presented in the following.

Concerning *Problem 2a*, Figure 3.10 shows the plots of Equation 3.54. Only the left "+" branch constitutes a valid locus, along which $C_{m,RMS}$ and

$P_{m,RMS}$ are zero. In Figure 3.10 the J_m parameter is modified to enhance the distance between k^* and k^{**}, that in reality are:

$$k^{**} = 3.5333 \text{ Nm/rad} \qquad k^* = 3.5348 \text{ Nm/rad}$$

Figures 3.11 and 3.12 show the plots of $C_{m,RMS}$ and $P_{m,RMS}$ in the $k-i$ plane and as 3D surfaces. Both the zero-torque-power locus $i_{opt,1}$ and the nonzero-torque-power locus $i_{opt,2}$ are shown, given by Equation 3.59.

As predicted by the equations previously derived, the required RMS motor torque and power can be zero for $0 < k < k^*$. For any fixed value of k in the range $k > k^*$ there always exists an optimum value for the transmission ratio, $i_{opt}(k)$, that minimizes $C_{m,RMS}$, while no such optima exist for $P_{m,RMS}$.

Figures 3.13a and 3.13b report, respectively, $C_{m,RMS}$ and $P_{m,RMS}$ as functions of i for three values of k. For $k = 0.9$ Nm/rad and $k = 3.05$ Nm/rad both $C_{m,RMS}$ and $P_{m,RMS}$ admit a zero. For $k = 80$ Nm/rad, no zero can be obtained for either $C_{m,RMS}$ or $P_{m,RMS}$, but $C_{m,RMS}$ admits an interior minimum, whereas $P_{m,RMS}$ doesn't.

Similarly, Figures 3.13c and 3.13d show, respectively, $C_{m,RMS}$ and $P_{m,RMS}$ as functions of k for three selected values of i: 5, 20 and 48.

Concerning *Problem 2b*, a global minimum exists for $C_{m,RMS}$, as given by Equation 3.61:

$$i_{opt} \approx 48 \qquad k_{opt} \approx 3.05 \text{ Nm/rad} \qquad C_{m,RMS} \approx 0.0296 \text{ Nm}$$

and a different global minimum exists for $P_{m,RMS}$:

$$i_{opt} \approx 22 \qquad k_{opt} \approx 1.84 \text{ Nm/rad} \qquad P_{m,RMS} \approx 3.3266 \text{ W}$$

The locus of optimum i as function of k, $i_{opt}(k)$ for $C_{m,RMS}$ and $P_{m,RMS}$ are shown in Figures 3.14 and 3.15. As shown, no zero exists for RMS motor torque and power. For any fixed value of k there always exist an optimum value of the transmission ratio $i_{opt}(k)$ minimizing $C_{m,RMS}$, whereas interior optima exist for $P_{m,RMS}$ only for small values of k.

A comparison analogous of that of Figure 3.13 can be found in Figure 3.16.

Again, the results underline the major influence of the load trajectory profile on both motor requirements and optimal transmission parameters.

Table 3.1: Numerical parameters used for numerical analysis

Inertial Parameters			
Motor inertia	J_{motor}	7.09×10^{-6}	Kgm^2
Wave Generator inertia	J_{WG}	4.90×10^{-6}	Kgm^2
Circular Spline inertia	J_{CS}	3.025×10^{-5}	Kgm^2
Flexible Spline inertia	J_{FS}	6.92×10^{-6}	Kgm^2
Input shaft inertia	$J_{INSHAFT}$	2.55×10^{-5}	Kgm^2
Output shaft inertia	$J_{OUTSHAFT}$	8.95×10^{-2}	Kgm^2
Spring shaft inertia	$J_{SPRINGSHAFT}$	5.002×10^{-4}	Kgm^2
Brake shaft inertia	J_{BRAKE}	5.1×10^{-3}	Kgm^2
SEA Derived Parameters			
J_m	$J_{motor} + J_{inshaft} + J_{WG}$	3.75×10^{-5}	Kgm^2
J_l	$J_{outshaft}$	8.95×10^{-2}	Kgm^2
J_g	$J_{FS} + J_{SPRINGSHAFT}$	5.07×10^{-4}	Kgm^2
DEA Derived Parameters			
J_m	$J_{motor} + J_{inshaft} + J_{WG}$	3.75×10^{-5}	Kgm^2
J_l	$J_{CS} + J_{OUTSHAFT}$	8.95×10^{-2}	Kgm^2
J_s	$J_{FS} + J_{BRAKE}$	5.1×10^{-3}	Kgm^2
Output Motion Data			
Angular motion span	A	3	rad
Movement duration	t_a	1	s

Chapter 4

DEA Prototype

In this chapter a prototype of an optimized Differential Elastic Actuator is presented. The actuator features an Harmonic Drive, a custom designed spring, a braking mechanism. Some major design choices are described.

4.1 Introduction

In order to test the validity of the procedure discussed in previous chapters, a prototype of compliant actuator was designed. The selected architecture was the DEA, employing an Harmonic Drive as differential transmission. The choice of a DEA instead of the more common SEA is due to multiple reasons.

First of all, there are far less DEA prototypes in the literature than SEAs, therefore this actuator offers new exploration possibilities in the field of compliant actuation.

Secondly, since only one end of the spring is moving, whereas the other is fixed to ground, it's easier to directly measure the spring deflection instead of obtaining such quantity indirectly from the measurement difference between the motor and the load encoders. Moreover, also the inertia distribution of the spring allows for better inertial properties since not the whole spring is moving during trajectory execution.

Table 4.1: Selected Beckhoff motor main technical characteristics

AM8112-1F21			
Nominal DC voltage [V]	48	Rated power [W]	170
Rated torque [Nm]	0.36	Peak torque [Nm]	1.36
Rated speed [min^{-1}]	4500	Max speed [min^{-1}]	10000
Peak current [A]	16.5	Rotor inertia [Kgm^2]	7.09×10^{-6}

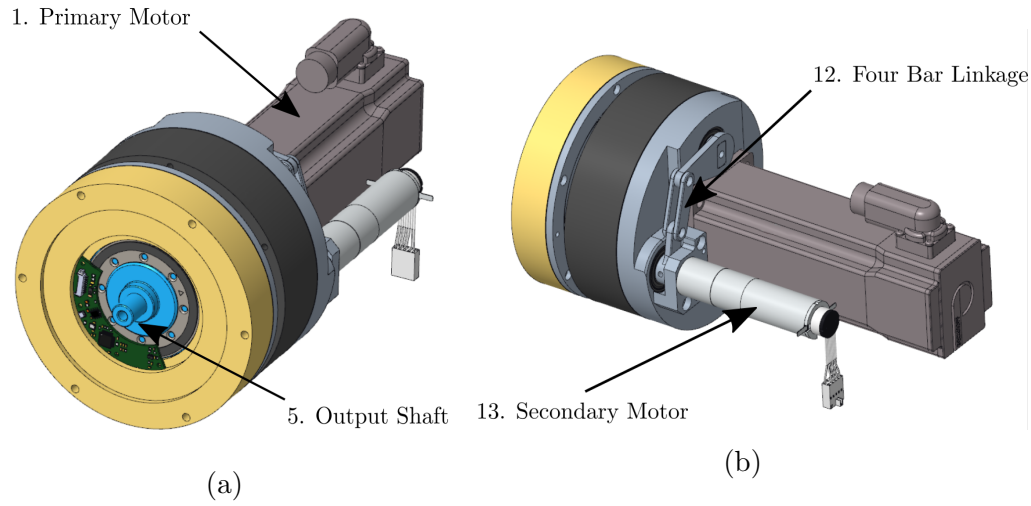

Figure 4.1: VDDEA: 3D view (a) front and (b) back of the proposed actuator.

In addition, the DEA architecture offers the possibility to introduce an external mechanism to alter the behavior of the spring element, similarly to the concepts of Variable Damping Actuators. Introducing a braking mechanism between the actuator's ground and the moving end of the spring, gives the possibility to transition from a DEA behavior to a RA behavior, whenever needed, completely bypassing the compliant element. Possibly, the secondary actuation mechanism would empower the actuator with the capability of controlling, to some extent, the degree of transition between the two configuration. The actuator will therefore behave similarly to a Variable Damping Actuator, implemented with a Differential Elastic architecture instead of the common Series Elastic one (VDDEA: Variable Damping Differential Elastic Actuator).

The 3D CAD drawing of the actuator can be seen in Figure 4.1 with the indication of the primary motor (1) that transmits motion towards the output shaft (5), and the secondary motor (13) that actuates the internal brake through the four-bar linkage (12).

The application of this actuator will be twofold:

- Two of these actuators will be devoted to control a planar five-bar linkage (5R). The 5R mechanism allows to test both high dynamic trajectories typical of pick-and-place applications and low dynamics movement typical of neurorehabilitation in post-stroke patients, where of course the ability to force-control and regulate the interaction with the human is of paramount importance.

- A single actuator will be tested with point-to-point trajectories typical

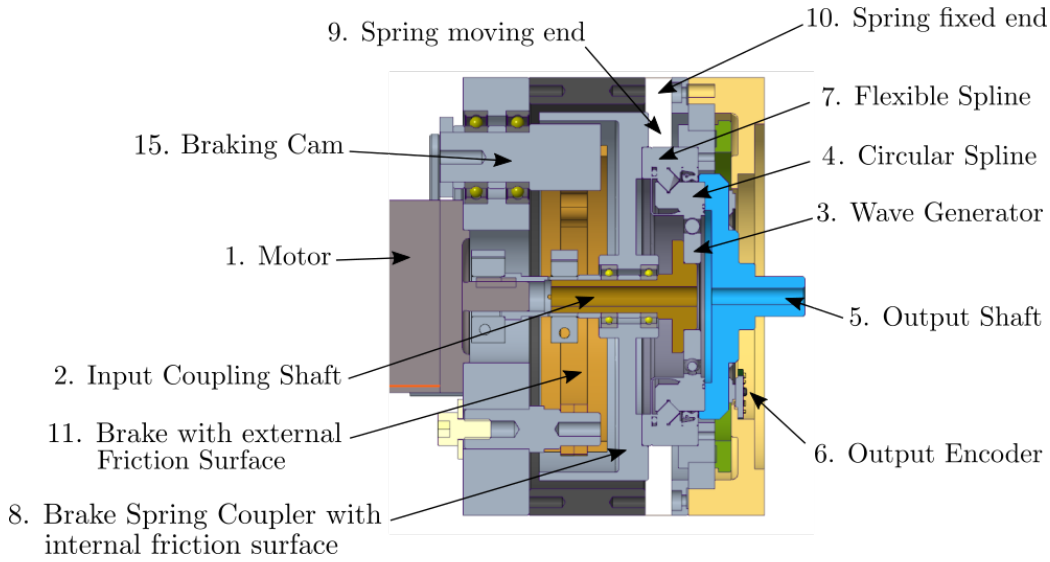

Figure 4.2: VDDEA: cross section of the actuator with all core elements.

of industrial automatic machines, to study the beneficial effects on efficiency and energy consumption of an optimally-design compliant actuator with respect to the traditional rigid actuator.

4.2 Description of the actuator's architecture

The cross section of the core of the actuator is presented in Figure 4.2. Referring to the numbering represented in Figure 4.2, we have that the selected primary motor (1) is a Beckhoff AM8112-1F21, whose main technical data are collected in Table 4.1. The motor's shaft is prolonged through an input coupling shaft (2) tied to the Harmonic Drive's Wave Generator (3). The selected reducer is the Harmonic Drive SHD-20-50-2SH, whose technical details are reported in Table 4.2. The Harmonic Drive has a reduction ratio

Table 4.2: Selected Harmonic Drive main technical characteristics

SHD-20-50-2SH			
Reduction Ratio	50	Max torque [Nm]	39
Max input speed [min^{-1}]	6500	Rated torque [Nm]	24
Rated input speed [min^{-1}]	3500	CS inertia [Kgm^2]	3.025×10^{-5}
External diameter [mm]	90	WG inertia [Kgm^2]	4.90×10^{-6}
Length [mm]	19	FS inertia [Kgm^2]	6.92×10^{-6}

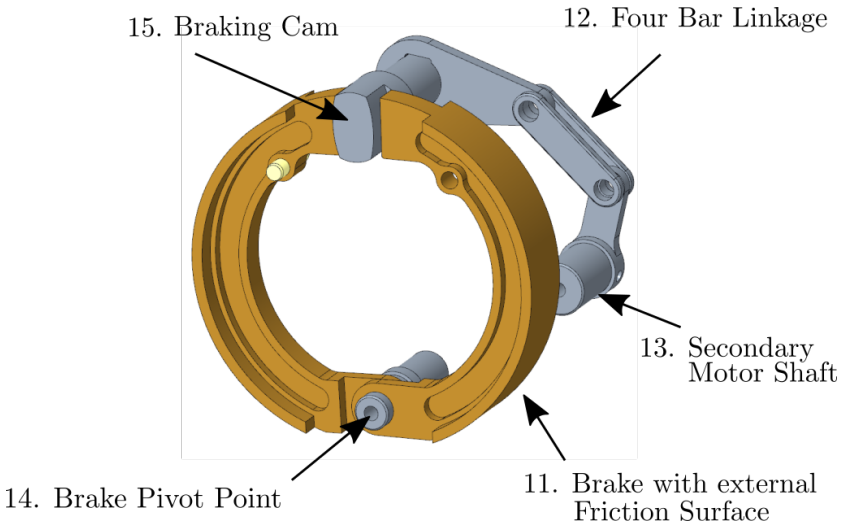

Figure 4.3: VDDEA: detail of the braking assembly

$i = 50$, and already incorporates a supporting bearing between the Flexible Spline and the Circular Spline. The output shaft (5) is linked directly to the Circular Spline (4). On the output shaft, a magnetic off-axis absolute encoder (6) provides feedback on the angular position of the load. The Flexible Spline (7) is connected on one side to an element that acts as brake-spring coupler (8). This element connects together multiple components: the transmission's Flexible Spline (7), the Spring's moving end (9) and offers a "cup" with internal friction surface, coupled with the brake's external Friction Surface (11). The other side of the Flexible Spline (7) is connected to the mechanical support of a second off-axis absolute magnetic encoder that provides feedback on the deflection of the spring, and is supported to ground through a bearing. The fixed end of the spring (10) is locked to ground via screws. The opening and closing of the brake (11) is governed by the braking cam (15).

A detailed view of the brake assembly is presented in figure 4.3. The secondary motor (13) actuates a four bar linkage (12), designed to operate in close proximity of a dead point configuration in order to maximize the input-output mechanical advantage. The rotation of the cam (15) makes the brake halves (11) open and contact the internal friction surfaces on (8), rotating around the pivot point (14).

4.3 Conclusions and future work

In this work a unified procedure for modeling elastic actuators and solving both the direct and inverse dynamic problem was presented. An important addition to the traditional modeling is not neglecting the self mass/inertia of the spring element, that in certain conditions can become non negligible with respect of the inertias of other mechanical components.

The generalized solution of the inverse dynamic problem has been used to perform the optimization of elastic actuators with respect to the traditional figures of merit $C_{m,RMS}$ and $P_{m,RMS}$, thus presenting a generalization of the traditional well known approach applied to 1-DOF actuators. Despite the complexity of the problem, which lends itself more to a task-specific numerical solution than to an analytical one, example study cases were presented both for SEAs and DEAs in two different application scenarios.

The optimization results were used as guidelines to design a novel VDDEA. The described actuator is currently under final design stages and preproduction of the mechanical components, in parallel with ordering of the commercial components.

One important aspect is the design of the spring element, that is going to be accomplished using laser-cutting, whereas the shape will be designed according to FEM simulations performed in ANSYS in order to obtain the desired optimal spring constant k. The actuator is designed in order to facilitate disassembling and reassembling of the spring component. This will allow to easily and quickly design and test new spring topologies, shapes and materials.

The actual effectiveness of the braking system in VDDEA needs to be experimentally proven, both in its "binary" "on-off" working mode (making the VDDEA function either as a RA or as a DEA), and its "analogic" working mode (making the VDDEA function as a VDA). An ad-hoc control algorithm needs to be developed for controlling the secondary motor of the VDDEA.

The effectiveness of the DEA architecture in force-controlled interaction tasks, such as human-machine interaction, needs to be assessed. The objective is to bring the technology in the field of human upper limb rehabilitation in the form of a 5R planar mechanism.

From a theoretical point of view, the optimization procedure outlined in Chapter 3 neglects the effect of the external torque $C_{ext}(t)$ and considers only the effect of the required motion trajectory $\theta_l(t)$. In real case scenarios, the external torque cannot be easily neglected, and the combined effect of both $C_{ext}(t)$ and $\theta_l(t)$ needs to be thoroughly analyzed.

Lastly, as seen while developing the numerical examples the optimization procedure's results are heavily affected by the selected motion law. An even

more generalized approach that abstracts from the imposed motion law, or maybe even brings the motion law in the optimization loop in order to suggest "best" trajectories to exploit even further the optimization, needs to be studied.

Bibliography

[1] R. McNeill Alexander. *Elastic Mechanisms in Animal Movement*. Cambridge University Press, 1988.

[2] Samuel K Au, Jeff Weber, and Hugh Herr. "Biomechanical design of a powered ankle-foot prosthesis". In: *2007 IEEE 10th International conference on rehabilitation robotics*. IEEE. 2007, pp. 298–303.

[3] Harrison L Bartlett, Brian E Lawson, and Michael Goldfarb. "Optimal transmission ratio selection for electric motor driven actuators with known output torque and motion trajectories". In: *Journal of Dynamic Systems, Measurement, and Control* 139.10 (2017).

[4] Ronald C. Rosenberg Dean C. Karnopp Donald L. Margolis. *System Dynamics: Modeling, Simulation, and Control of Mechatronic Systems*. Wiley, 2012.

[5] Xiaomin Dong et al. "Research on variable stiffness and damping magnetorheological actuator for robot joint". In: *International Conference on Intelligent Robotics and Applications*. Springer. 2017, pp. 109–119.

[6] S. H. Drake. "Using compliance in lieu of sensory feed-back for automatic assembly". Ph.D. dissertation. MIT, 1977.

[7] H Giberti, S Cinquemani, and G Legnani. "Effects of transmission mechanical characteristics on the choice of a motor-reducer". In: *Mechatronics* 20.5 (2010), pp. 604–610.

[8] Hermes Giberti, Simone Cinquemani, and Giovanni Legnani. "A practical approach to the selection of the motor-reducer unit in electric drive systems". In: *Mechanics based design of structures and machines* 39.3 (2011), pp. 303–319.

[9] Matthew M. Williamson Gill A. Pratt. "Series elastic actuators". In: *IEEE International Conference on Intelligent Robots and Systems* (1995).

[10] Russel D. Howard. "Joint and Actuator Design for Enhanced Stability in Robotic Force Control". Ph.D. thesis. MIT, 1990.

[11] Matteo Laffranchi et al. "Development and control of a series elastic actuator equipped with a semi active friction damper for human friendly robots". In: *Robotics and Autonomous Systems* 62.12 (2014), pp. 1827–1836.

[12] Michel Lauria et al. "Differential elastic actuator for robotic interaction tasks". In: *2008 IEEE International Conference on Robotics and Automation*. IEEE. 2008, pp. 3606–3611.

[13] Chan Lee and Sehoon Oh. "Configuration and performance analysis of a compact planetary geared elastic actuator". In: *IECON 2016-42nd Annual Conference of the IEEE Industrial Electronics Society*. IEEE. 2016, pp. 6391–6396.

[14] Chan Lee et al. "Generalization of series elastic actuator configurations and dynamic behavior comparison". In: *Actuators*. Vol. 6. 3. Multidisciplinary Digital Publishing Institute. 2017, p. 26.

[15] Giovanni Legnani et al. *Meccanica degli azionamenti vol. 1-Azionamenti elettrici*. 2009.

[16] Theodore E Milner and Caroline Cloutier. "Damping of the wrist joint during voluntary movement". In: *Experimental brain research* 122.3 (1998), pp. 309–317.

[17] Erick A Padilla-Garcia et al. "Concurrent optimization on the powertrain of robot manipulators for optimal motor selection and control in a point-to-point trajectory planning". In: *Advances in Mechanical Engineering* 9.12 (2017), p. 1687814017747368.

[18] Nicholas Paine, Sehoon Oh, and Luis Sentis. "Design and control considerations for high-performance series elastic actuators". In: *IEEE/ASME Transactions on Mechatronics* 19.3 (2013), pp. 1080–1091.

[19] Nicholas Paine et al. "Actuator control for the NASA-JSC valkyrie humanoid robot: A decoupled dynamics approach for torque control of series elastic robots". In: *Journal of field robotics* 32.3 (2015), pp. 378–396.

[20] Jerry Pratt and Gill Pratt. *Intuitive control of a planar bipedal walking robot*. ICRA, 1998.

[21] Siavash Rezazadeh and Jonathan W Hurst. "On the optimal selection of motors and transmissions for electromechanical and robotic systems". In: *2014 IEEE/RSJ international conference on intelligent robots and systems*. IEEE. 2014, pp. 4605–4611.

[22] David W Robinson et al. "Series elastic actuator development for a biomimetic walking robot". In: *1999 IEEE/ASME International Conference on Advanced Intelligent Mechatronics (Cat. No. 99TH8399)*. IEEE. 1999, pp. 561–568.

[23] Rodney A. Brooks Cynthia Breazeal Matthew Marjanovic Brian Scassellati and Matthew Williamson. *The Cog Project: Building a Humanoid Robot*. Springer-Verlag, 1999.

[24] WP Seering. "On the Drive Systems for High-Performance Machines". In: *Journal of Mechanisms, Transmissions, and Automation in Design* 106 (1984), p. 103.

[25] Herman J Van de Straete et al. "Servo motor selection criterion for mechatronic applications". In: *IEEE/ASME Transactions on mechatronics* 3.1 (1998), pp. 43–50.

[26] Stefano Toxiri et al. "A parallel-elastic actuator for a torque-controlled back-support exoskeleton". In: *IEEE Robotics and Automation Letters* 3.1 (2017), pp. 492–499.

[27] V Van Geffen. *A study of friction models and friction compensation*. 2009.

[28] Bram Vanderborght et al. "Variable impedance actuators: A review". In: *Robotics and autonomous systems* 61.12 (2013), pp. 1601–1614.

[29] Tom Verstraten et al. "Series and parallel elastic actuation: Impact of natural dynamics on power and energy consumption". In: *Mechanism and Machine Theory* 102 (2016), pp. 232–246.

[30] Matthew M. Williamson. "Series elastic actuators". Master's thesis. MIT, 1995.